PCCP

On the mechanism of soot formation

Journal:	*Physical Chemistry Chemical Physics*
Manuscript ID	CP-ART-01-2020-000116.R1
Article Type:	Paper
Date Submitted by the Author:	07-Feb-2020
Complete List of Authors:	Frenklach, Michael; University of California at Berkeley, Department of Mechanical Engineering Mebel, Alexander; Florida International University, Chemistry and Biochemistry

Physical Chemistry Chemical Physics

On the mechanism of soot nucleation†

Michael Frenklach*[a] and Alexander M. Mebel*[b,c]

The mechanism of carbon particulate (soot) inception has been a subject of numerous studies and debates. The article begins with a critical review of the prior proposals, proceeds to the analysis of factors enabling the development of a meaningful nucleation flux, and then introduces new ideas that lead to the fulfillment of these requirements. In the new proposal, a rotationally-activated dimer is formed in collision of aromatic molecule and radical, the two react during the lifetime of the dimer to form a stable, doubly-bonded bridge between them, with the reaction rooted in a five-member ring present on the molecule edge. Several such reactions were examined theoretically and a most promising one generated a measurable nucleation flux. Consistency of the proposed model with known aspects of soot particle nanostructure is discussed. The foundation of the new model is fundamentally the H-Abstraction-Carbon-Addition (HACA) mechanism with the reaction affinity enhanced by rotational excitation.

1 Introduction

Soot inception in fossil-fuel combustion has been a subject of studies for over a century. Adverse health effects and negative impact on the Earth environment are the most cited reasons for the interest and motivation in developing fundamental understanding and ability to model the formation of soot and its properties. The science of the phenomena is fascinating in its own right: crossing boundaries of and bridging several disciplines, calling for and benefiting from synergy of experiment and theory, discovering remarkable patterns of material self-organization, and having implications to contemporary topics in atmospheric chemistry, astrophysics, and climate change. Over the past few decades, many aspects of the phenomena have been interpreted in fundamental terms with one of the remaining unknowns of, and hence increasing emphasis on, the actual "act" of particle inception.

The accumulating experimental and theoretical evidence seems to bring the community to consensus that polycyclic aromatic hydrocarbons (PAH) are the molecular precursors to soot particles, as delineated by Haynes and Wagner,[1,2] and the key question is what type of processes are responsible for the transition from gaseous PAH to "solid" carbonaceous particles, referred to as soot nucleation. Before addressing this question, it is imperative to examine the fundamentals of the PAH growth itself. Not only does this understanding help in identification of the actual molecular candidates for the nucleation, but also, as

we show here, it equips one with pertinent theoretical constraints.

Growth of PAHs in size, starting with benzene, encounters a thermodynamic barrier at the two-three-ring level,[3,4] caused by the decrease in entropy in molecular addition steps.[5] Many of the carbon-addition reactions at this stage run in reverse as a result of this. The molecular growth follows the path of the increase in reaction affinity,[6] by the mechanism termed HACA, hydrogen-abstraction-carbon-addition,[3,5,7] which stands for repetitive sequence of two primary steps: activation of aromatic molecule by hydrogen abstraction followed by the carbon (acetylene) addition to the radical formed. The increase in reaction affinity, and hence in the flux of PAH growth, is attributed to the abundance (super-equilibrium) of H atoms in the region of nucleation in the first, activation step, and formation of particular stable aromatic products, referred to as islands of stability[3] or stabilomers,[4] in the acetylene-addition step, all accompanied by increases in entropy due to the formation of H_2 and H, respectively, in these two principle reaction steps.[5] Recent re-evaluation[8] of the energetics and thermochemistry of the associated reactions reaffirms the initial discovery of HACA.[5]

It is imperative to stress again[5,9] that the defining feature of the HACA mechanism is the kinetic-thermodynamic coupling and not necessarily the nature of the carbon growth species, as remains misunderstood and misrepresented by many authors. This being said, it is also important to realize that under soot-forming conditions in combustion environments acetylene emerges as the most prominent growth species due to its thermal stability, and hence abundance, along with its reaction affinity to radical addition. The argument for acetylene goes all the way back to Porter,[10] who proposed an early acetylene-growth model of soot formation. Not unrelated to nucleation, the predominance of acetylene was demonstrated to be the primary source of soot surface growth in experimental studies of Harris and Weiner.[11] Clearly, species other than acetylene,

[a.] Department of Mechanical Engineering, University of California, Berkeley, California 94720, USA.
[b.] Department of Chemistry and Biochemistry, Florida International University, Miami, Florida 33199, USA.
[c.] Samara National Research University, Samara 443086, Russia

including aromatics themselves,[12-15] can propagate polymerization-type[16,17] aromatic growth[5] and propositions of various growth species have kept recurring.[18-25] However, detailed kinetic modeling has demonstrated the emergence of acetylene-driven HACA under combustion (and high-temperature pyrolysis) conditions.[12-14,22,24] Also, the first step of HACA, activation of an aromatic site, can be not just abstraction, but also H addition.[26] Thus, HACA can be more generally thought of as an acronym for *H-Activated-Carbon-Addition* featured by the underlying kinetic-thermodynamic coupling, where "H-Activated" implies "H-Abstraction", "H-Addition" or even "H-migration".

There are several consequences to the present subject of nucleation stemming from the HACA model of growth. First, the "winning" pathways are those with higher reaction affinity, meaning those having not just fast forward rates but also slow reverse rates, and thus smaller entropy loss. For PAH growth it turns out that periodic re-activation of the growing molecule provides a more efficient pathway to growth than seemingly a "more direct" path of radical growth advocated by Homann and co-workers[27-29] and recently by Johansson *et al.*[30] Second, the first significant island of stability "pulling" the HACA sequence forward is acenaphthylene (A2R5 in our notation[13]). The significance of this, noted from the very start[3] and reinforced in subsequent theoretical[26,31-35] and kinetics[36-38] studies, is that the formation of PAHs along the HACA sequence is accompanied by the formation of five-member rings. By now, the presence of five-member aromatic rings in precursor PAH and young soot particles has been established in experimental studies.[39-51] Third, the major island of stability, the one that is primarily responsible for overcoming the two-three-ring thermodynamic barrier, turned out to be pyrene (A4).[3] It is one of the reasons that the inception of particles was proposed to be initiated by pyrene.[52] In support of this HACA-founded prediction, two recent analyses of large sets of experimental data concluded that "regardless of the physical and chemical processes involved in the young soot formation and growth, A4 and smaller species serve as the initial stable reactants"[53] and "large PAHs … are not required to nucleate soot … the PAHs involved in the process have mass below 200-225 u".[50] Other recent studies, however, concluded that inception begins with 10-ring[54] or 16-ring[49,55] PAH.

Once pyrene-level aromatics are formed, they continue to grow in size via HACA reacting at its edges. This growth, termed chemical growth, can account for the evolution of soot mass but not for soot particle size and its structure.[52,56] It has long been recognized[57-59] and continuously reaffirmed[48,49,60-68] that soot particles are not just amorphous carbon networks but composed of disordered PAH clusters, thus indicating the role of PAH-cluster and cluster-cluster collisions in their formation. The extent of chemical versus collisional growth was suggested to depend on conditions, such as temperature and carbon-precursor density.[5] Moreover, it was suggested[5] that the two pathways are not different mechanisms,[69] but represent the two regimes of a common mechanism, and some combination of the two forming aromatic-aliphatic-linked-hydrocarbons (AALH). The specific nature of the underlying interactions has

taken the center stage of the present quest by the combustion-research community.

Frenklach and co-workers[52,70] suggested that "starting with a prescribed size," PAHs begin clustering. The numerical model,[52,71] constructed in harmony[70] with the knowledge of particle internal structure, PAH-precursor hypothesis, and surface growth and oxidation, assumed that the PAH clustering is due to physical forces. It was recognized,[52] however, that the thermodynamic stability of small PAH clusters, called into attention by Miller *et al.*[72] and later attested to by others,[73-75] is alarmingly low, which led to questioning possible forces holding PAH and their clusters together. Two such possible factors were suggested:[52] ionic forces and crosslinking.
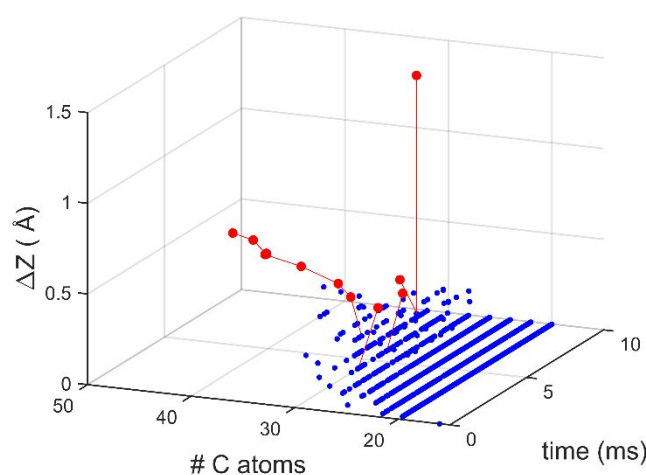
Fig. 1 Predicted cPAHs appearance with KMC model[36,37,76] for the conditions of a burner-stabilized stagnation flame:[77] 16.3% C_2H_4–23.7% O_2–Ar, cold gas velocity 8.0 cm/s, and burner-to-stagnation surface separation 0.8 cm. The gas-phase composition was computed with the ABF model.[15] 1000 KMC runs were performed starting at 1300 K position of the flame with a pyrene substrate. The curved PAH instances are plotted as red dots and the planar PAH ones as blue dots. The red lines connect the cPAHs instances formed in the same KMC runs. The curvature, ΔZ, was defined as the difference between extreme out-of-plane C atoms of the PAH structure.

The ionic forces, long advocated by Calcote,[78,79] were experimentally[80] and theoretically[5,81-83] argued to be an unlikely explanation for particle inception. Recently, a possible role of ions in soot particle nucleation was given another opportunity. Kraft and co-workers have noticed that curved PAHs (cPAHs) are polarized,[84] which leads to higher binding energies with other PAHs and even higher with chemi-ions present in flames,[85] and the latter could then induce particle nucleation.[86] While this phenomenon can be viable, as the authors proposed,[86,87] there are several considerations suggesting that such a mechanism could not be general. First, the enhancement in binding energy may not be sufficient to overcome the reversibility of PAH dimerization at soot-forming conditions, as will be discussed in the next section. Second, while the presence of chemi-ions may be adequate in flames, in oxygen-free environments, such as pyrolysis, their abundance is much lower. For instance, shock-tube experiments demonstrated[88] that soot formation from toluene does not exhibit a significant change, and certainly not an increase, with the addition of small amounts of oxygen,

2 | *Phys. Chem. Chem. Phys.* 2020, **00**, 1-3

This journal is © The Royal Society of Chemistry 20xx

whereas the presence of oxygen would have dramatically increased the amount of ions.[78,89,90] Finally, the present knowledge of reaction chemistry indicates that the curved PAHs do not appear immediately with the formation of A4.[36] This is exemplified in Fig. 1, which shows that significantly curved PAHs appeared only in 2 out of 1000 kinetic Monte-Carlo (KMC) simulations of the soot-forming region of one of the well-studied flames,[77,91,92] and even that happened toward the end of that region; at the same time, ample production of planar PAHs continued throughout the simulated region. It is pertinent to mention that the experimental evidence from shock-tube testing the effect of oxygen addition on soot formation also suggests that oxygen-induced reactions, whatever they may be,[93,94] cannot be the key to soot nucleation, as the experiments show the same intensity of soot inception with and without oxygen addition.

Particle inception via bridged PAHs seems, at the moment, to be a more likely alternative. Recently reported high-resolution atomic force microscopy images[48,51] provide a definitive evidence for the existence of bridged PAH structures in the inception region of a flame. Such structures would be consistent with the observation of aliphatic signals[48,95,96] and with the suggestion of Homann that at some size a planar-formed biaryl would bend forming a bi-layered structure.[29,40,41] Theoretical inquiries into the PAH bridging, however, face difficulties to fully account for particle inception.

Investigation of the energetics of PAH cross-linking identified such possibilities, one being an ethylene bridging two aromatic.[97] One must consider, however, that the formation of such aliphatic bridges may be kinetically unstable. Let us explain this by the following example. One of the proposals for soot formation invoked polyacetylenes.[27,28,98] Indeed, if an argument could be made for acetylene because of its thermodynamic stability and ability to add (to radicals) then polyacetylenes should be next in line. Homann and Wagner[28] outlined such a possible pathway and Krestinin[98] developed a reaction network for it. However, Krestinin's reaction network was composed of a "minimal" set of irreversible building-up steps. Adding other conceivable reactions, such as

$$R\text{-}C\equiv C\text{-}C\equiv C\text{-}R' + H \rightarrow R\text{-}C=CH\text{-}C\equiv C\text{-}R' \rightarrow R\text{-}C\equiv CH + \bullet C\equiv C\text{-}R' \quad (1)$$
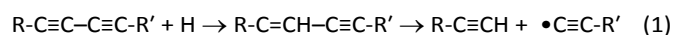
prevents the polyacetylene route from efficient molecular growth.[99] Likewise, a bridged aromatic structure can fall apart by H abstraction (or H addition) and β-scission

$$Aryl\text{-}CH=CH\text{-}Aryl' + H \underset{-H_2}{\longrightarrow} Aryl\text{-}C=CH\text{-}Aryl' \rightarrow Aryl\text{-}C\equiv CH + \bullet Aryl' \quad (2)$$
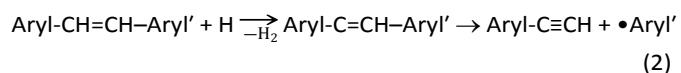
Bridged aromatic structures were generated in recent reactive molecular-dynamics (MD) simulation.[100,101] However, these simulations were performed with starting aromatic-monomer densities on the order of 10^{20} cm^{-3}, whereas those observed in flame nucleation zones are on the order of 10^{12} cm^{-3}. Densities exaggerated to such an extent must distort the kinetic-thermodynamic coupling of the molecular interactions at flame conditions.

Two recent proposals assumed soot nucleation to proceed through bridged aromatics.[30,102] Both efforts confronted the thermodynamic instability of PAH dimerization, both invoked elements of HACA as means to overcome it, and, yet, both offered little specifics to accept either proposal as a viable solution to the problem

Kholghy et al.[102] employed generic kinetics for the PAH-PAH bond formation, and found that the reversibility of PAH dimerization must be relaxed to attain meaningful rates of nucleation. Specifically, these authors suggested that such a break in reversibility should take place following reversible formation of dimers by "strong chemical bond formation between dimers", reminiscent of mechanisms discussed by Miller et al.,[72] and that "All PAHs do contribute to nucleation, however small PAHs, such as A1 and A1C2 … contribute substantially." It is hard to imagine physico-chemical processes that would explain the abrupt switch, suggested by Kholghy et al.,[102] from reversible formation of dimers to their irreversible combination. Irrespective of the physical considerations, numerical analysis presented in Sections 2 and 3 cannot support such a model.

Johansson et al.[30] described a list of possible reactions leading to molecular growth, building on resonance-stabilized radicals. Increased molecular stability through electron delocalization is well known,[103] and a possible role of resonance-stabilized structures in soot formation was probably first invoked by Glassman,[104] suggesting 1,3-butadiene "to be the essential precursor to soot." On similar grounds, the remarkable stability of C_3H_3 radical was suggested[105] to explain shock-tube observations that allene produces soot at levels similar to those of benzene;[13] indeed, propargyl recombination[106] has been shown time and again to dominate the formation of the first aromatic ring under many (if not most) flame conditions. Furthermore, that early analysis[105] concluded to suggest that "The most efficient 'building blocks' for the formation of soot embryos … seem to be species … which have conjugated molecular configuration" and that "the incipient soot formation … must follow the route of consecutive production of the conjugated reactive structures." One needs to consider, however, that the much lower abundance of such radicals as compared to acetylene limits the growth rates with these species to make a difference, as was discussed for the case of propargyl.[5] While the later steps of Johansson et al.'s proposal[30] are reminiscent of HACA, the initial steps of the reaction sequence suggest a continuous line of addition steps, which is likely to be kinetically disadvantageous as follows from the discussion of HACA. Also, some of the initial steps seem unlikely on the basis of available calculations and experiments. For example, the $C_5H_5 + C_2H_2$ reaction postulated to produce vinylcyclopentadienyl radical was actually predicted to form 1-ethynylcyclopentadiene and fulveneallene as the main products at typical combustion temperatures, with vinylcyclopentadienyl and possibly tropyl being only minor significant intermediates.[107,108] Similarly, the reaction of indenyl with acetylene does not form vinylindene radicals but instead produces 1-ethynylindene and maybe benzotropyl, according to the recent experiments in a pyrolytical microreactor and

This journal is © The Royal Society of Chemistry 20xx

Phys. Chem. Chem. Phys. 2020, **00**, 1-3 | **3**

calculations.[109] In summary, the mechanistic details of the molecular first stage of Johansson *et al.*[30] may not be valid and need to be better understood in terms of the kinetics and equilibrium. The proposed mechanisms critically rely on H abstractions from intermediates, which are not likely to be sufficiently stable to survive long enough to collide with an H-abstractor.

There is one more aspect that needs to be considered: non-equilibrium phenomena of PAH collisions. Miller[110] noticed that the stability of PAH dimers is increased by considering that one of the colliding PAH molecules orbits the other. Attempting to reproduce this phenomena through MD simulations, Schuetz and Frenklach[111] indeed observed rotation but of emerging *internal* rotors of the colliding PAH. Further MD simulations indicated that the dimer lifetime increases with the PAH mass but not necessary with the presence of aliphatic chains,[112] radical sites,[112] or oxygen.[113,114] The calculations showed a pattern of rotation-to-vibration energy transfer, indicative of Boltzmann non-equilibrium.[111,112,115] To capture this pattern requires that the movement of all atoms be taken into account. Such calculations are time consuming and do not allow the collection of reliable statistics on PAH dimerization.[86,111,112,115] An approximate transition-state-theory (TST) treatment indicated that a forming dimer could survive for sufficiently long times,[111] but that would require an assumption of essentially all internal rotors being activated and remain active during the time period of collisions with other PAHs. The latter is a rather strong assumption, possible but probably not likely to occur.

We thus face a dilemma. Present theoretical knowledge cannot fully account for soot particle inception. On the one hand, numerical simulations of flames seem to require, in order to match the appearance of soot, the initiating PAH to be of the size of pyrene with dimerization treated as an irreversible process, perhaps lowered by a factor not more than an order of magnitude.[15,92,116] On the other hand, present understanding cannot fully account for the apparent irreversibility of such a process. The present study is an attempt to resolve this by identifying a conceivable bridged aromatic structure whose formation and survival withstands the kinetic and thermodynamic constraints of the nucleation regime.

We begin the analysis by examining in Section 2 the conditions to be satisfied for attaining practical nucleation fluxes and extend these results in Section 3 to confirm that purely-collisional (physical) nucleation of PAHs is hampered by the low thermodynamic stability of initial PAH clusters. We then turn, in Section 4, to reaction-based (chemical) nucleation, investigate the energetics and kinetics of several reaction candidates, and test the nucleation flux for the most promising one. The outlook for the entire soot inception process is presented in Section 5. Principle conclusions are summarized in Section 6.

2 Kinetics-thermodynamics coupling of nucleation

We consider a simple model of nucleation,

$$\xrightarrow{r_0} P_1 \xrightleftharpoons{P_1} P_2 \xrightleftharpoons{P_1} P_3 \xrightleftharpoons{P_1} \cdots \xrightleftharpoons{P_1} P_m \#(3)$$
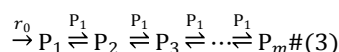
where P_1 is a monomer (say, pyrene), P_2 is its dimer, P_3 trimer, and so on, and r_0 is the rate of monomer formation. This model is the kinetic description of homogeneous nucleation.[117-119] It represents reversible addition of a monomer where the reversibility declines with the increase in polymer size, reaching a state, called critical, when the monomer addition becomes essentially irreversible.

The present study is concerned with the very initial stages of soot particle inception and model (3) fundamentally represents such a process. Indeed, at the start of nucleation, the system is dominated by the abundance of the monomer (*e.g.*, pyrene) and hence the kinetics is dominated by the first monomer-addition steps before it transforms to the full particle dynamics.[120]

The kinetic equations for Model (3) are

$$\frac{d[P_1]}{dt} = r_0 - \sum_{i=1}^{m-1} r_i$$

$$\frac{d[P_{i+1}]}{dt} = r_i - r_{i+1}, \ i = 1, 2, ..., m-1, \quad \#(4)$$

$$\frac{d[P_m]}{dt} = r_{m-1}$$

$$r_i = k_{f,i}[P_1][P_i] - k_{r,i}[P_{i+1}],$$

where t is the reaction time, $[P_i]$ is the concentrations of P_i, all starting at zero except possibly of the monomer, P_1, $k_{f,i}$ and $k_{r,i}$ are the rate coefficients of the forward and reverse directions, respectively, of the ith monomer addition step, with the corresponding equilibrium constants defined as $K_i = k_{f,i}/k_{r,i}$ for $i = 1, 2, ..., m-1$.

To expose general kinetic-thermodynamic features of system (3), we bring eqs (4) to a nondimensionalized form by making two assumptions, inconsequential in the present context: the monomer remains at a constant concentration, and the forward rate constants are the same for all monomer addition steps. Introducing then the following definitions

$$n_i = \frac{[P_i]}{[P_1]}, \qquad i = 2, 3, ..., m, \quad \#(5)$$

$$d\tau = k_f[P_1] \, dt \, ,$$

eqs (4) are transformed into

$$\frac{dn_i}{d\tau} = r_i - r_{i+1}$$

$$\frac{dn_m}{d\tau} = r_{m-1} \quad \#(6)$$

$$r_i = n_i - \frac{1}{\mathcal{K}i} n_{i+1}, \quad i = 1, 2, ..., m-1,$$

where

$$\mathcal{K}i = \frac{k_{f,i}[P_1]}{k_{r,i}} = K_i[P_1] \#(7)$$

is the "reduced" equilibrium constant of ith monomer-addition

step or, in other words, the equilibrium constant of pseudo first-order growth step,

$$P_i \underset{k_{r,i}}{\overset{k_{f,i}[P_1]}{\rightleftharpoons}} P_{i+1} . \#(8)$$
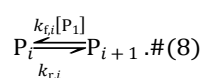
Differential equations (6) were solved numerically using the Matlab suit of ODE solvers.[121] The initial/boundary conditions were $n_1 = 1$ and $n_i(\tau = 0) = 0$ for $i = 2, 3, ..., m$. The value of m was set equal to 100, large enough not to affect the computed distribution of n_i, as was checked numerically by doubling the value of m. The numerical integration of eqs (6) was carried out from $\tau = 0$ to $\tau = 10$, covering the time period of soot inception in a flame examined in the next sections (*i.e.*, $k_f \sim 10^{-13}$ cm^{-3}s^{-1}, pyrene mole fraction $\sim 10^{-6}$, and $\Delta t \sim 10$ ms). The nucleation flux was judged by the computed distribution of P_i as compared to that of the irreversible growth. The latter was obtained in solving eqs (6) with $k_{r,i} = 0$ for all i and denoted hereafter as $\mathcal{K} = \infty$.

The first series of runs was performed with all $\mathcal{K}_i$ set equal to same value. In this way, model (6) has only one parameter and it is straightforward to examine the trends. The numerical results, depicted in Fig. 2(a,b,c), indicate that the value of $\mathcal{K} = 1$ demarcates attainment of a meaningful nucleation flux. Indeed, at $\mathcal{K} = 1$, the concentrations of the initial P's are significant, showing a sizable nucleation flux. At higher values of $\mathcal{K}$, the P_i distribution rapidly moves toward the irreversible case and approaches it for $\mathcal{K} = 10$. At $\mathcal{K} < 1$, the nucleation flux rapidly declines and is essentially diminished at $\mathcal{K} < 0.1$.
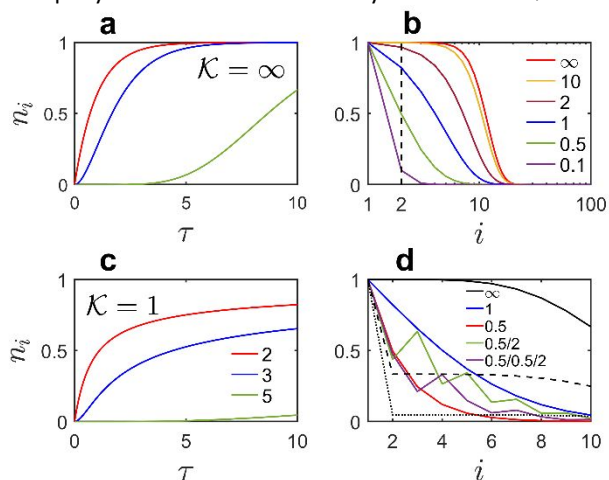
Fig. 2 Normalized concentrations of P_i computed with model (6). Panels **a** and **c** display the time evolution of dimer, trimer, and pentamer. The final P$_i$ distributions, at $\tau = 10$, computed with different values of $\mathcal{K}$ are displayed in panels **b** and **d**, where the values of n_i for discrete i's are connected by lines to guide the eye. The dash and dotted lines in panel **d** designate cases when the first reversible step, with $\mathcal{K}_1 = 0.5$ and $\mathcal{K}_1 = 0.05$, respectively, was followed by all subsequent steps set irreversible.

The next series of runs with model (6) was carried out by alternating the values of $\mathcal{K}$ and comparing the resulting P_i distributions against those computed with constant $\mathcal{K}$. The results are presented in Fig. 2d. The first alternating case, shown in green and identified by the "0.5/2" legend, is produced with $\mathcal{K}_i = 0.5$ and $\mathcal{K}_{i+1} = 2$, for $i = 1, 3, 5, etc.$ As can be seen in Fig. 2d, the computed P_i concentrations are bracketed by the constant-$\mathcal{K}$ lines, $\mathcal{K} = 0.5$ and $\mathcal{K} = 1$, but tending toward the latter one with the increase in i. On the other hand, with the alternation that repeats the lower $\mathcal{K}$ value twice before switching to the higher value—the case, designated by the "0.5/0.5/2" legend in Fig. 2d, with $\mathcal{K}_i = \mathcal{K}_{i+1} = 0.5$ and $\mathcal{K}_{i+2} = 2$, for $i = 1, 4, 7, etc.$—the resulting P_i distribution tends toward the lower-value case of $\mathcal{K} = 0.5$.

The alternating-$\mathcal{K}$ results underscore the kinetics-thermodynamics coupling, the one underlying and distinguishing the HACA model discussed in Section 1. They expose the difference of the repetitive scheme of H-abstraction followed by carbon addition (*i.e.*, HACA[3,5]) from that of H-abstraction followed by *several* carbon addition steps (present, *e.g.*, in the models of Homann and co-workers,[27-29] Bittner and Howard,[39] and Johansson *et al.*[30]). Also to be noticed is that the convergence of the "0.5/2" results to those of constant $\mathcal{K} = 1$ is not coincidental. Indeed, the more reversible first step of the alternating-$\mathcal{K}$ growth sequence can be assumed partially equilibrated, with $n_2/n_1 \approx \mathcal{K}_1$, and hence the rate of the second step is given as

$$r_2 = n_2 - \frac{1}{\mathcal{K}_2}n_3 = \mathcal{K}_1\left(n_1 - \frac{1}{\mathcal{K}_1\mathcal{K}_2}n_3\right), \#(9)$$

implying that the net rate of such a two-step growth sequence is governed by the product of the respective $\mathcal{K}$'s,

$$\mathcal{K}_{1-2} = \mathcal{K}_1\mathcal{K}_2, \#(10)$$

and, hence, the effects of "pushing" by H-abstraction and "pulling" by islands of stability, the defining features of HACA,[3,5] are both to increase the value of $\mathcal{K}$ of the HACA cycle. The latter observation will be further addressed in Section 5, where it forms the basis for the pursuit of answers to the mechanism of soot nucleation.

One more set of numerical tests was performed with the first reversible step followed by irreversible steps. Two such tests are reported in Fig. 2d, designated by the dashed and dotted lines, with $\mathcal{K}_1 = 0.5$ and $\mathcal{K}_1 = 0.05$, respectively, followed by all subsequent steps set irreversible. The results indicate that the dimer concentration, n_2, drops to about the value of $\mathcal{K}_1$ with the remaining P_i's first staying at the same level and then dropping down. Two immediate conclusions can be drown from these results. First, the meaningful nucleation flux is determined by the reduced equilibrium constant of the very first step, $\mathcal{K}_1$, and becomes negligibly small for its low values. And second, if reversibility of the first step prevents development of a meaningful nucleation flux, so will be any strategy of gradual increase in $\mathcal{K}_i$'s of subsequent steps. In other words, for a highly reversible first step, such as dimerization of pyrene, invoking irreversible steps for subsequent growth, as suggested by Kholghy *et al.*,[102] will not lead to soot nucleation. This conclusion will be confirmed in realistic flame simulations presented in the next section.

This journal is © The Royal Society of Chemistry 20xx

Phys. Chem. Chem. Phys. 2020, **00**, 1-3 | **5**

3 Physical nucleation

We consider here model (3) where the product of monomer addition, P_{i+1} in eq (8), is held together due to physical (van der Waals) forces, without forming covalent bonds between P_1 and P_i. The kinetics were solved in the explicit form, eqs (4), for the conditions of one of the well-studied burner-stabilized stagnation flames:[77,92] 16.3% C_2H_4–23.7% O_2–Ar, cold gas velocity 8.0 cm/s, and burner-to-stagnation surface separation 0.8 cm. The gas-phase composition was computed using Cantera[122] with the ABF model.[15] The computed flame temperature, concentration profile of pyrene, assumed to be the monomer, and its rate of formation, r_0, were supplied into a Matlab code of eqs (4). The latter were solved from the flame time of 1 ms, corresponding to the flame temperature of 1412 K and the pyrene mole fraction of 1.2×10^{-8}, for the duration of 10 ms, with the zero initial concentrations set for the rest of the P_i's. The values of $k_{f,i}$, the frequencies of PAH collisions, were computed by eq 10.18 of Frenklach and Wang,[71] and those of $k_{r,i}$ were calculated using equilibrium constants, K_p, reported by Totton *et al.*[75]

The runs were performed with $k_{r,i}$ calculated using constant values of K_p, as it will become clear from the results that the conclusions reached would not be affected by a nuanced strategy in their assignment, especially considering the temperature range variation of only 300 K. The runs with $K_p = 1 \times 10^{-4}$ bar^{-1} for pyrene produced no nucleation flux, consistent with the earlier conclusions,[73-75] and so did those with 1×10^{-3} bar^{-1} for coronene and ovalene. These results conform to the respective values of $\mathcal{K} \sim 10^{-10}$ and $\mathcal{K} \sim 10^{-9}$, which are dramatically below the condition of $\mathcal{K} \sim 1$ for attaining a meaningful flux. Indeed, the flux begins to develop at K_p approaching the range of 10^5–10^6 bar^{-1}, corresponding to $\mathcal{K} \sim 0.1$.

Variation of K_p with temperature[73,75] and PAH size,[123] amounting at most to one to two orders of magnitude increase in K_p over the simulated flame zone, is far from closing the 8 to 10 orders of magnitude gap in the K_p values. Neither the increase in binding energy due to PAH curvature[86] nor due to PAH π bonding[124] (tested with one of the more promising radicals, acepyrenyl, discussed in the next section), is sufficient to cover this gap. An analogous outcome happens with continuing the growth of P_2 through irreversible self-collisions. Finally, considering the development of internal rotation upon PAH collision, the K_p values of 10^5–10^6 bar^{-1} would require activation of 4 such degrees of freedom,[111] which seems to be unlikely. We thus must conclude against purely physical nucleation of PAHs as the underlying mechanism of soot particle inception and look at reaction-based alternatives.

4 Bridge-forming nucleation

We explore now bridge-forming reactions that may lead to the meaningful nucleation fluxes. We begin by outlining, in Subsection 4.1, a set of requirements that such reactions must satisfy, follow with a preliminary, scouting examination of

possibilities in Subsection 4.2, proceed with a detailed analysis of candidate reactions in Subsection 4.3, and conclude by modeling the nucleation outcome of most promising bridge-forming reactions in Subsection 4.4.

4.1. Requirements

The present knowledge, reviewed in Section 1, leads to a set of requirements for possible reaction candidates to satisfy:

A). The overall nucleation rate must be sufficiently close to that of the irreversible physical nucleation.

B). The reaction product must survive until the next growth step.

C). The bridge structure must induce the development of a non-planar shape.

Requirement A is motivated by the body of modeling results accumulated thus far,[15,92] demonstrating that the assumption of irreversible physical nucleation starting with pyrene,[52] perhaps reduced by a factor no lower than an order of magnitude,[92] is sufficient (or required) to reproduce the time evolution of soot in better-understood laminar premixed flames. Requirement B, placing the obvious constraint on the cluster lifetime, stipulates that the rates of the reverse reaction and those of other product destruction reactions must be smaller than the rate of the next growth step. Requirement C should assure that the growth sequence will lead to a stacked PAH structure, as evidenced by the experimental observations.[42,49,57,61-63,65,68]

4.2. Preliminary exploration

The first set of bridge-forming reactions we examined are those between molecular PAHs, *i.e.*, when neither one of the colliding PAH is a radical. One promising candidate in this set is a 4-center bridge, *i.e.* a "doubly-linked" bridge, illustrated in Fig. 3 for two acenaphthylenes. While satisfying requirements B and C, the relatively high energy barriers computed for this class of reactions do not meet requirement A; for instance, the barrier for the recombination of two acenaphthylenes is computed to be at least 51.5 kcal/mol, consistent with this pericyclic reaction being formally symmetry-forbidden according to the Woodward-Hoffmann rules.

4-center bridge connecting two acenaphthalenes

E-bridge connecting two naphthalenes

C-C covalent bond bridge

1,2-ethylene bridge

1,1-ethylene bridge

E-bridge connecting two pyrenes
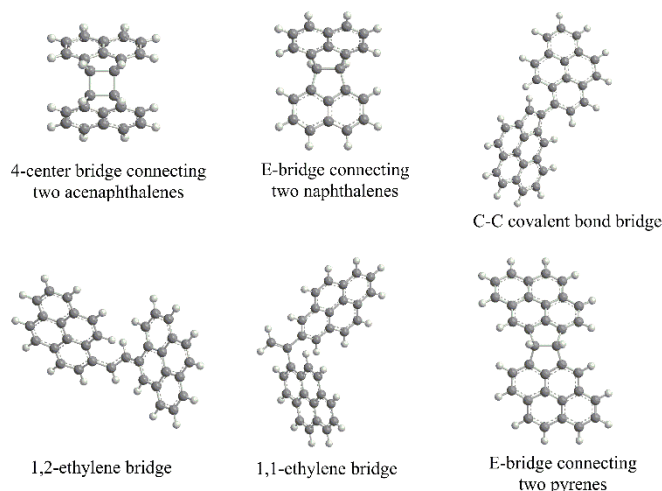
Fig. 3 Molecular structures illustrating bridged PAHs.

6 | *Phys. Chem. Chem. Phys.* 2020, **00**, 1-3

This journal is © The Royal Society of Chemistry 20xx

We also considered another type of a doubly-linked bridge referred to as "E-bridge" (Fig. 3) and studied, as an example for its formation, the reaction between naphthalene and acenaphthylene. The reaction mechanism is similar to well-known Diels-Alder-type dimerization of cyclopentadiene and involves the addition of the five-member ring of acenaphthylene to the zigzag edge of naphthalene (Fig. 4). According to our density functional (DFT) calculations, the reaction first forms an intermediate with two five-member rings connecting two naphthalene moieties, which is followed by H_2 elimination, with two H atoms leaving from the attacked zigzag edge. The final product can be described as naphthalene-2R5-naphthalene (or, briefly, A2-2R5-A2), with two naphthalenes connected via a double bridge made of two fused five-member rings. The reaction appeared to be 8–14 kcal/mol exoergic, but the calculated barriers along the pathway, 67–78 and 85–94 kcal/mol relative to acenaphthylene + naphthalene for the first and second steps, respectively, are too high for the reaction to be feasible.
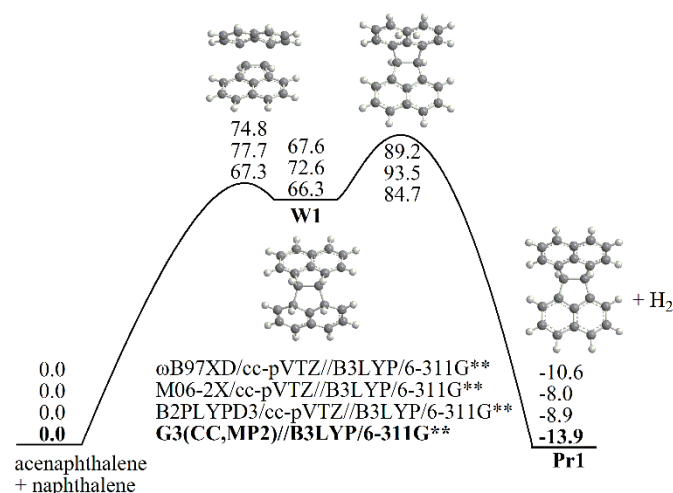
Fig. 4 Potential energy diagram for the formation of E-bridge in molecular addition of acenaphthalene and naphthalene. The energy values are in kcal/mol.

From the radical-molecule reactions, we did not consider directly-linked PAHs, like biphenyl. They do not pass requirements B and C, as they are typically not sufficiently stable at temperatures of soot nucleation and when they do, they rapidly "reinforce" the PAH-PAH connection, and thus the planar structure, by adding C_2H_2, like forming phenanthrene in the case of biphenyl.[12-14,125] We also did not consider bridges linking PAHs through "singly-linked" aliphatics, like the 1,2-ethylene bridge in Fig. 3; such structures are kinetically unstable, as illustrated by reaction 2 discussed in Section 1, and thus violate requirement B.

Our primary focus, therefore, was on a doubly-linked E-bridge, which will be examined in more detail next. Such bridges are formed in reactions of five-member rings present on PAH edges. One of the attractive reactants is the one having a radical formed on the edge five-member ring (*i.e.*, −CH−CH$_2$−); hence we also examined reactions of its formation and decomposition. The specific reactants chosen for the present study are pyrene, acepyrene (A4R5), and acepyrenyl radicals.

4.3. Reactions forming doubly-linked bridges

4.3.1. Methodology. Potential energy surfaces of the reactions considered in the present study were first mapped via geometry optimization and vibrational frequency calculations at the DFT B3LYP/6-311G** level[126,127] for the reactants, intermediates, transition states, and products. Single-point energies of the most important structures were refined using the G3(MP2,CC) composite scheme, which normally provides chemically accurate reaction energies, although its performance for barrier heights may be less reliable.[128,129] Generally, G3(MP2,CC) energies are expected to be more accurate than those computed by current DFT methods. However, since G3(MP2,CC) calculations for such systems as acepyrenyl + pyrene are extremely demanding in terms of computing resources, we were able to perform them only for few structures. In addition, single point energies were also recalculated using three different modern density functionals, "kinetic" M06-2X,[130] ωB97XD,[131] and doubly-hybrid B2PLYPD3,[132-134] all with Dunning's cc-pVTZ basis set.[135] The results of the DFT calculations were compared with those of G3(MP2,CC) where available. In general, the B2PLYPD3 approach has shown the best agreement with G3(MP2,CC) in terms of relative energies. Gaussian 09[136] and MOLPRO 2010[137] packages were employed in the DFT and ab initio calculations. Next, the energetics and molecular parameters were utilized in Rice-Ramsperger-Kassel-Marcus Master Equation (RRKM-ME) calculations[138] of temperature- and pressure-dependent rate constants using the MESS package.[139] The Rigid-Rotor, Harmonic-Oscillator (RRHO) model was utilized in the calculations of the densities of states and partition functions for the local minima and the number of states for the transition states. We used collision parameters derived in the literature for similar systems; the Lennard-Jones parameters ε and σ for hydrocarbons were taken from Wang and Frenklach[140] and those for N_2 bath gas from Vishnyakov *et al.*[141,142] Collisional energy transfer in ME was described using the "exponential down" model,[143] where the temperature dependence of the range parameter α for the deactivating wing of the energy transfer function is expressed as $\alpha(T) = \alpha_{300}(T/300)^n$, with $n = 0.85$ and $\alpha_{300} = 247$ cm^{-1} proposed by Jasper and Miller as "universal" values for hydrocarbons.[144] Energies in RRKM-ME calculation were taken from G3(MP2,CC) calculations where available or from B2PLYPD3 otherwise.

4.3.2. Acepyrenyl formation and decomposition reactions. The acepyrenyl radical (denoted A4-R5-H in Fig. 5) possesses a high degree of electron delocalization, thus promising high reactivity. This radical can be produced by H addition to the five-member ring in acepyrene via a low barrier. All DFT and G3(MP2,CC) calculations consistently predict the barrier height in the 0.7–3.1 kcal/mol range, with the most reliable G3(MP2,CC) value being 2.0 kcal/mol. The strength of the newly formed C–H bond in A4-R5-H is computed to be 41.7 kcal/mol but the scatter in the DFT results is larger than for the barrier height, from 39.9 kcal/mol at the B2PLYPD3 level to 48.2 at ωB97XD; the B2PLYPD3 result is the closest to the G3(MP2,CC) value. RRKM-ME calculations at 1 atm give the rate constant for

the formation of acepyrenyl from 8.6×10^{-12} cm^3 molecule^{-1} s^{-1} at 500 K to 5.4×10^{-11} cm^3 molecule^{-1} s^{-1} at 1125 K, then falling to 3.1×10^{-11} cm^3 molecule^{-1} s^{-1} at 1375 K. The calculations indicate that A4-R5-H does not exist at temperatures above 1375 K at 1 atm as it immediately equilibrates with A4-R5 + H. At higher pressures, the acepyrenyl radical may persist up to higher temperatures, 1500 and 1650 K at 3 and 10 atm, respectively. The rate constant for the formation of A4-R5-H somewhat grows with pressure, with its maximal values being 6.1 and

7.3×10^{-11} cm^3 molecule^{-1} s^{-1} at 3 and 10 atm, respectively, both occurring at 1250 K. The rate constant for the reverse dissociation of A4-R5-H to A4-R5 + H rapidly increases with temperature, from ~6×10^4 s^{-1} at 1000 K to the maximal values of 1.3×10^7 s^{-1} (1375 K), 5.0×10^7 s^{-1} (1500 K), and 2.1×10^8 s^{-1} (1650 K) at 1, 3, and 10 atm, respectively, showing also a noticeable increasing trend with pressure. Thus, at the temperatures of interest the acepyrenyl may exist on a submicrosecond timescale.
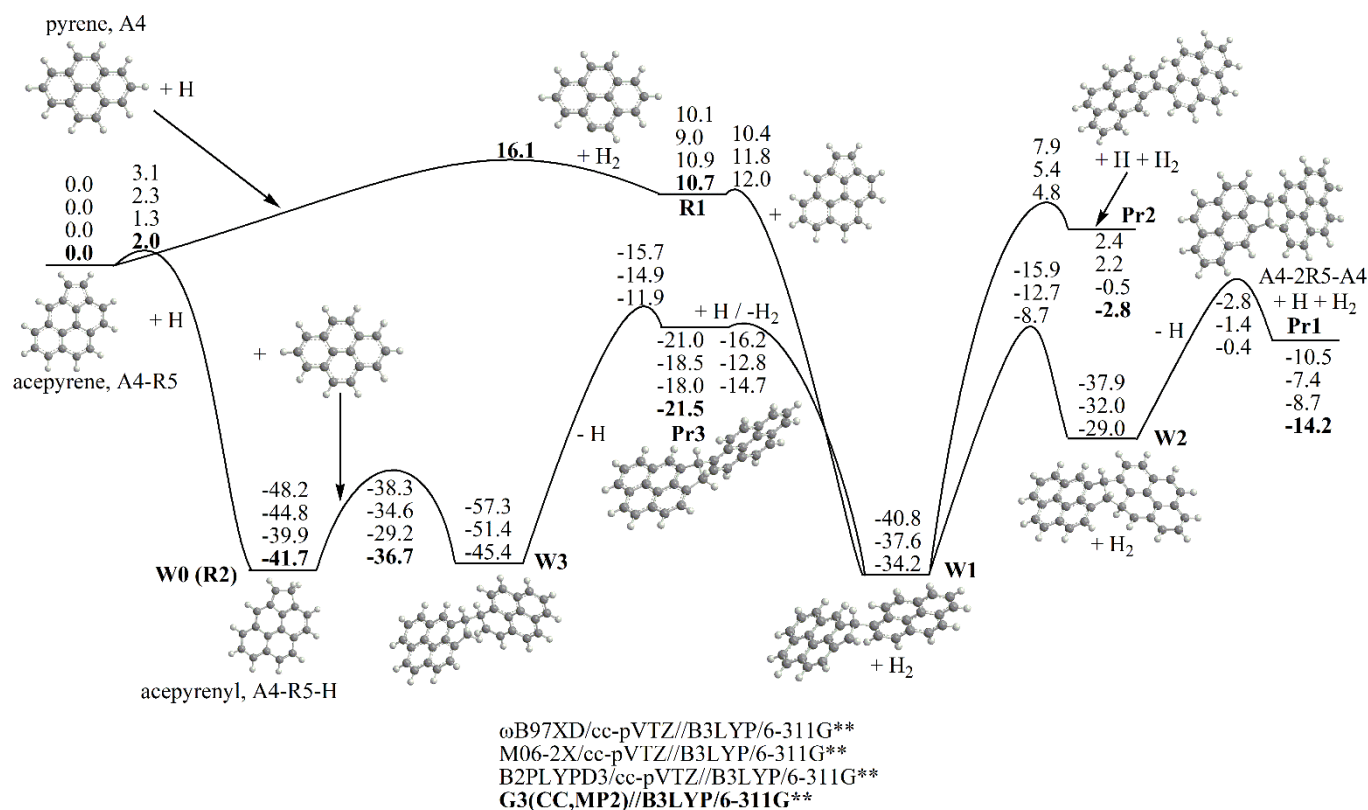
Fig. 5 Potential energy diagram for the formation of E-bridge in radical-molecule reactions. The energy values are in kcal/mol.

4.3.3. Acepyrenyl-pyrene reaction. If acepyrenyl survives long enough, it may enter into bimolecular reactions with other PAH molecules, such as pyrene. A bimolecular reaction would be able to compete with unimolecular decomposition of A4-R5-H back to A4-R5 + H only if it has a high rate constant and the concentration of the reaction counterpart is high enough. Here we considered the reaction of acepyrenyl with pyrene as a potential source of the E-bridged structure connecting two acepyrenes, A4-2R5-A4. The calculated PES for the A4-R5-H + A4 reaction and some consequent processes is illustrated in Fig. 5. The reaction begins with pyrene addition to the five-member ring of acepyrenyl to form intermediate W3. The barrier for this addition varies from 16.5 kcal/mol at B3LYP to ~10 kcal/mol at the other DFT levels of theory, but the G3(MP2,CC) method gives the lowest value of 5.0 kcal/mol. The covalently bound intermediate W3 is exothermic with respect to the A4-R5-H + A4 reactants by 5.5–9.1 kcal/mol at all DFT levels except B3LYP, at which it is 3.3 kcal/mol endothermic. W3 can in principle isomerize and dissociate to the E-bridged A4-2R5-A4 structure after removal of three H atoms (or H$_2$ and

H) and closure of a second five-member ring at the double bridge. We first looked for H$_2$ elimination from W3 but the search of a corresponding transition state failed. Instead, W3 prefers to eliminate an H by forming the product denoted Pr3 in Fig. 5 via a barrier in the 33.5–41.6 kcal/mol range. The A4-R5-H + A4 → Pr3 + H reaction appears to be endothermic by 21.9–36.6 kcal/mol at the DFT levels of theory and by 20.2 kcal/mol at G3(MP2,CC), where the result with the B2PLYPD3 functional, 21.9 kcal/mol, agrees closest with the G3(MP2,CC) value. If the Pr3 closed-shell molecule can be formed, it can be easily reactivated again by H abstraction from the CH$_2$ group in the five-member ring; the respective barrier is only 3.3 kcal/mol at B2PLYPD3 and not too different at the other levels of theory. The H abstraction step, Pr3 + H → W1 + H$_2$, is exothermic by 16.2 kcal/mol at B2PLYPD3. Finally, W1 can decompose to A4-2R5-A4 (Pr1) via a two-step process involving first, closure of a second five-member ring at the bridge (W2) and second, elimination of an extra hydrogen from the former pyrene moiety. The alternative decomposition processes of W1 involve direct H elimination with ring closure producing Pr2 in which

8 | *Phys. Chem. Chem. Phys.* 2020, **00**, 1-3

This journal is © The Royal Society of Chemistry 20xx

acepyrene and pyrene are linked by a single C–C covalent bond, or cleavage of the linking C–C bond forming acepyrene + pyrenyl radical (R1). However, the calculated PES clearly shows that the decomposition of W1 to Pr1 + H is preferred over those to Pr2 + H and acepyrene + pyrenyl according to the product energies and barrier heights. Can this three-step elementary reaction sequence,

$$A4\text{-}R5\text{-}H + A4 \rightleftarrows Pr3 + H$$

$$Pr3 + H \rightleftarrows W1 + H_2$$

$$W1 \rightarrow A4\text{-}2R5\text{-}A4 \ (Pr1) + H$$
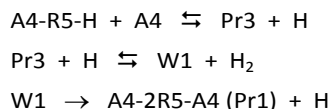
actually produce the E-bridged structure A4-2R5-A4 under the prevailing conditions of soot nucleation? The answer to this question can be found through kinetics calculations.

Figure 6a displays rate constants of the acepyrenyl + pyrene (R2) $\rightleftarrows$ Pr3 + H reaction in the forward and reverse directions along with the direct H abstraction Pr3 + H $\rightarrow$ W1 + H$_2$ reaction, which competes with the H addition to Pr3 leading back to acepyrenyl + pyrene. Obviously, for A4-R5-H + A4 (R2) $\rightleftarrows$ Pr3 + H the reaction in reverse direction is several orders of magnitude faster than in the forward direction. Nevertheless, the three-step reaction sequence outlined above has a chance to move forward because the H abstraction channel for Pr3 + H is faster (by factors in the 2.5–2.9 range) than the H addition channel. Once W1 is formed, it can undergo fast unimolecular decomposition, preferably A4-2R5-A4 (Pr1) + H (see Fig. 6b). At 1500 K, the calculated W1 → Pr1 + H rate constant is as high as 9.2×10^6 s^{-1}, factors of 2.3 and 2.6 higher than the rate constants for the competing channels to Pr2 + H and acepyrene + pyrenyl (R1), respectively. Above 1500 K, W1 no longer exists and equilibrates preferably with Pr1 + H but fractionally also with Pr2 + H and R1. Summarizing, the three-step reaction sequence (actually four-step, including the initial addition of an H atom to acepyrene) can in principle result in the formation of A4-2R5-A4 but the overall rate will be controlled by the low concentration of the acepyrenyl radical A4-R5-H, which appears to be rather unstable above 1400 K, and hence the slow A4-R5-H + A4 → Pr3 + H step. This violates requirement A, which was confirmed by detailed calculations similar to those in Section 4.4.
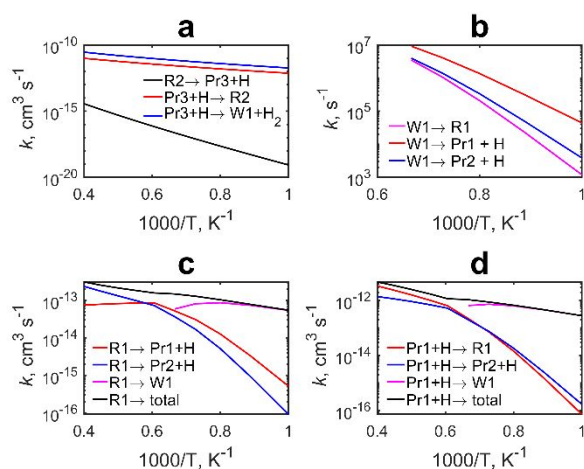
Another possibility to consider is first to have the five-member ring in acepyrenyl opened via a β-scission process, to move the radical site to the side-chain and to make the resulting species to react with pyrene and thus to connect two pyrene moieties with ethylene bridge (Fig. 7). However, our calculations show that these reactions are not favorable and are not likely to occur. For instance, the ring opening process in acepyrenyl (W0) requires a high barrier of 52.1 kcal/mol. Next, the intermediate W4 can isomerize to W5 by H migration from CH in the side-chain to the ring over a 22.3 kcal/mol barrier. The intermediate W5 with a –CH–CH$_2$– radical attached to pyrene lies only 14.3 kcal/mol lower in energy than acepyrene + H, compared to 41.7 kcal/mol for acepyrenyl. Kinetic calculations show that the rate constant to form collisionally stabilized W5 from acepyrene + H is 3-to-4 orders of magnitude lower than that to form W0. In principle, if W5 survives, it may react with pyrene to produce the ethylene-bridged product Pr4 via a two-step process involving a C–C bond formation followed H elimination from the pyrene moiety. The W5 + pyrene → Pr4 + H reaction is slightly endothermic, by 2.8 kcal/mol, and has the highest barrier of 17.0 kcal/mol (B2PLYPD3). The calculated rate constant in the reverse direction in the 1400–1600 K temperature range is more than two orders of magnitude higher than that in the forward direction. Therefore, the formation of the ethylene-bridged structure is highly unlikely as it violates requirements A and B and hence this nucleation pathway can be safely ruled out.
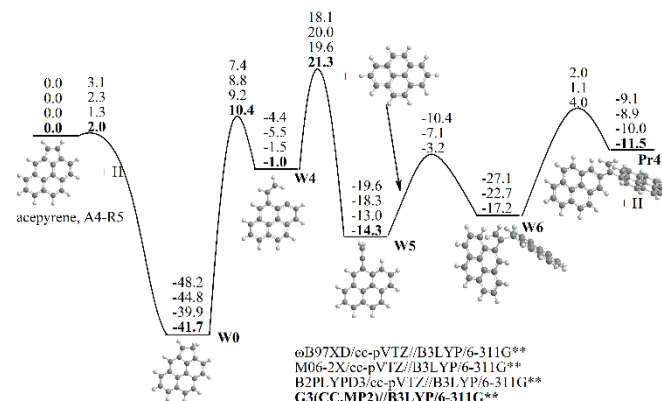
Fig. 7 Potential energy diagram for the formation of ethylene bridge. The energy values are in kcal/mol.

4.3.4. Acepyrene-pyrenyl reaction. As seen in the acepyrenyl-pyrene reaction system discussed above, the intermediate W1, a precursor of the E-bridged A4-2R5-A4 molecule, can be alternatively produced via addition of acepyrene to the pyrenyl radical. According to the computed PES (Fig. 5), the barrier for this addition step is 0.3–2.8 kcal/mol at various DFT levels; we consider the B2PLYPD3 value of 1.1 kcal/mol as the most trustworthy. W1 resides in a relatively deep potential well of 41.5–50.9 kcal/mol and can decompose by directly splitting an H atom forming Pr2 + H or by isomerizing to W2 via five-member ring closure and then eliminating H and producing Pr1. The highest barriers on the two competing pathways are evaluated as 39.0–48.7 and 33.8–40.7 kcal/mol, respectively, at different DFT levels, all of them consistently showing the

Fig. 6 Rate constant computed for the reaction system shown in Fig 5.

This journal is © The Royal Society of Chemistry 20xx

Phys. Chem. Chem. Phys. 2020, **00**, 1-3 | **9**

energetic preference of the Pr1 + H channel. At 1 atm W1 ceases to exist at T > 1500 K as it fully equilibrates with bimolecular products. In the 1400–1500 K temperature range W1 can be collisionally stabilized; however, the rate constant for its unimolecular dissociation to R1, Pr1, and Pr2 exceeds 10^6 s^{-1}. If the rate constant for a potential bimolecular reaction, H addition to W1, is in the range of the kinetic limit, ~10^{-10} cm^3 molecule^{-1} s^{-1}, for hydrogen addition to be competitive, the concentration of H atoms should be ~10^{16} molecule cm^3 corresponding to a mole fraction of ~0.002 at 1500 K and 1 atm, which is an order of magnitude higher than that in the flame we considered in the present study. The overall exothermicities for the acepyrene + pyrenyl → Pr1 + H/Pr2 + H reactions are computed as 24.9 and 13.5 kcal/mol at the most reliable G3(MP2,CC) level of theory. Again, the B2PLYPD3 method generally gives closest results to the G3(MP2,CC) "standard". Clearly, the acepyrene + pyrenyl → E-bridge + H reaction, which we represent as

$$A4R5 + A4\bullet \rightarrow A4\text{-}2R5\text{-}A4 + H , \qquad (11)$$

seems to be kinetically favorable and pyrenyl itself can be readily produced by direct H abstraction from pyrene (Fig. 5).

Let us now consider the calculated reaction rate constants in the forward and reverse directions. Figure 6c illustrates forward rate constants at 1 atm. First of all, the rate constants for acepyrene + pyrenyl are much larger than those for acepyrenyl + pyrene → Pr3 + H (Fig. 6a). At low temperatures, the reaction is dominated by collisional stabilization of W1, which however does not exist above 1500 K and, as discussed above, preferably dissociates to Pr1 + H. The formation of Pr1 + H via a well-skipping mechanism becomes favorable above 1500 K; however, as temperature increases, the Pr2 + H product takes over Pr1 + H above 1700 K. Due to the entropic preference of the direct H loss from W1, there exists only a narrow range of temperatures where the formation of the E-bridged A4-2R5-A4 structure dominates. Figure 6(d) shows rate constants of individual channels for the reverse, Pr1 + H reaction. Here, again at T < 1500 K, the reaction predominantly produces collisionally stabilized W1, which as we know would prefer to dissociate to back to Pr1 + H. At higher temperatures R1 becomes the favorable product. The reverse Pr1 + H → acepyrene + pyrenyl reaction becomes faster than the forward reaction above ~1200 K. Nevertheless, the equilibrium constant between A4-2R5-A4 + H and acepyrene + pyrenyl maintains significant values of 0.24–0.08 in the 1375–1650 K temperature range. Also, the production of Pr2 becomes preferable over the production of Pr1 at T > 1700 K at 1 atm (Fig. 6c). However, Pr2 is less stable as compared to Pr1 in the entire 1400–1800 K temperature range as the equilibrium constant K_{eq}(R1-Pr1) exceeds K_{eq}(R1-Pr2) by a factor of 3.2 to 1.1 and, accordingly, the equilibrium constant K_{eq}(Pr1-Pr2) is in the 3.2-1.1 range. Both Pr1 and Pr2 may contribute to nucleation, but the E-bridged structure more so. Furthermore, subsequent H abstraction from the E-bridge in Pr1 can make the two pentagonal cross link observed experimentally,[51] which corroborates the proposed mechanism. Altogether, this makes

us to consider the acepyrene + pyrenyl reaction as a viable candidate for a prototype soot nucleation step.

The rate coefficients calculated for reactions discussed above are reported in Table S1 of ESI.†

4.4. Nucleation kinetics with the bridging reaction

We now turn to the calculation of the nucleation flux for model (3) with each mass-growth step, $P_i \rightleftharpoons P_{i+1}$, assumed to be a two-step HACA sequence,

$$P_i + H \rightleftharpoons P_i\bullet + H_2 \#(Ia)$$

$$P_i\bullet + H \rightarrow P_i \qquad \#(Ib)$$

$$P_i\bullet + P_1 \rightleftharpoons P_{i+1} + H , \#(II)$$
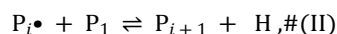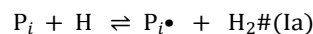
where step (I), composed of reactions (Ia) and (Ib), is the "pushing" activation(de-activation) of PAH cluster P_i through H abstraction (H-addition) and step (II) is the "pulling" carbon addition. Reaction (Ia) is the H-abstraction from a zigzag C–H site of the aromatic edge, P_1 is the monomer PAH with a five-member ring (e.g., acepyrene, A4R5), and reaction (II) is the E-bridge formation, eq (11), *but taking place in rotationally-activated collision* of $P_i\bullet$ and P_1.

Assuming reaction (II) to proceed with the rate coefficient reported in Section 4.3.4 for the acepyrene-pyrenyl reaction does not produce sufficient nucleation flux. Still, in collision of two PAHs we need to consider the development of internal rotation,[111,112,115] which emerges regardless of whether the collision occurs between two molecules or a molecule and a radical.[112] As discussed in Section 1, to overcome the thermodynamic instability of the formed physically-bound PAH dimer, essentially all internal rotors need to be active, deemed unlikely. However, partially activated internal rotation may be sufficient if stable covalent bonds can be forming during the lifetime of the rotational dimer. We reason as follows.

The computed MD trajectories[111,112] showed that during rotational interaction of the PAH molecules, their edge sites are "bumping" into each other on the time scale of about 0.1 to 1 ps. Multiplying this rotational collision frequency by the collision-theory efficiency of a reaction (i.e., reaction probability) estimates the frequency of the reaction in the (non-equilibrium) rotational setting. The reaction probability of reaction (11) above 1400 K is about 1×10^{-4}, making the reaction frequency under the rotationally-activated setting on the order of 10^{12}–$10^{13}\times10^{-4} = 10^8$–$10^9$ s^{-1}. These values translate to the required lifetime of the rotational adduct on the order of 10^{-9}–10^{-8} s, suggesting 2 to 3 internal rotors need to be activated,[111] a reasonable interpretation of the MD simulations.[111,112] It is pertinent to mention that reactions with high barriers and hence lower forward rates cannot meet this requirement.

We thus suggest that the activation of internal rotation creates "collisional events" between the edges of the rotating PAH that offer the opportunity for reaction to take place. It is similar to the mobile precursor mechanism of gas-surface reactions,[145] where weak physical attraction forces (e.g., van der Waals) trap the incident gaseous reactant in a bouncing trajectory that may lead to chemical bonding with an active (radical) site of the surface. Somewhat analogously to this gas-surface mechanism, the initial encounter of two PAHs, due to

10 | *Phys. Chem. Chem. Phys.* 2020, **00**, 1-3

This journal is © The Royal Society of Chemistry 20xx

the emerging internal rotation, is followed by their edges repeatedly bumping into each other until they either form a covalent bond or fly apart. The likelihood of the bond formation is determined by the probability of a specific reaction to ensue during the time period brought about by the repeated encounters of the corresponding sites. This time period is increased with additional forces acting between colliding PAHs, such as electrostatic[123] or π-π,[124] which in turn increases the likelihood of the reaction. The attractive forces increase with the size[123] and possible curvature[85,86] of the colliding PAHs. It is imperative to note that the reaction event in this scenario is the outcome of the initial encounter of the two PAHs and hence its overall kinetic rate is determined by the collision rate of the incoming PAHs.

Following these considerations, the forward rate of reaction step (II) was set equal to the PAH collision frequency, as done for the physical nucleation in Section 3; i.e., $k_{f,i}^{II} = \beta_{i,1}^{II}$, where $\beta_{i,1}^{II}$ is the collision efficiency of reaction (11). Its reverse rate was computed with the rate coefficient computed in Section 4.3.4 for the acepyrene-pyrenyl reaction. We assigned rates of the forward and reverse directions of step (II) separately because it is not an elementary reaction but a sequence of the PAH-edge rotationally-induced collisions followed by a chemical reaction. It is also important that the absolute value of the reverse rate is lower than that of the H-abstraction of aliphatic and aromatic C–H bonds thus confirming the required survival of the E-bridged PAH dimer (and larger clusters).

The per-site reaction rate coefficient for reaction (Ia) and its reverse were taken from our recent study[146] and that of reaction (Ib) from Harding et al.[147] The forward rate of reaction (Ia) was calculated by multiplying its per-site rate coefficient by the number of available for reaction (Ia) sites on the outer edges of the PAH cluster, P_i; for P_1 assumed to be pyrene, there are 8×2 = 16 such sites on each P_i for $i > 1$.

The kinetic simulations were performed for the same flame as the one used in the analysis of the physical nucleation in Section 3, with the computed flame temperature, rate of pyrene formation, and concentration profiles of H and H_2 supplied into the Matlab code solving the corresponding differential equations. The Matlab simulations also included the PAH growth in the flame zone; the average PAH size computed for the same flame conditions but in the KMC simulations (Fig. 1) is increased by 4 carbon atoms at the end of the simulation period of 10 ms.

The computed in the described manner PAH distribution is presented in Fig. 8, where it is compared to the PAH distribution obtained for the irreversible case of the physical nucleation in Section 3. Inspection of the results indicates that the distribution computed with model (I)-(II) is comparable to that of the irreversible case multiplied by 0.1, still indicating a measurable flux. The latter result is congruous with the reduced equilibrium constant of model (I)-(II),

$$\mathcal{K}_{I\text{-}II} = \mathcal{K}_I \mathcal{K}_{II} = \frac{k_f^{Ia}[H]}{k_r^{Ia}[H_2] + k_f^{Ib}[H]} \frac{k_f^{II}[P_1]}{k_r^{II}[H]}, \#(12)$$

similarly to the general case analyzed with model (3) in Section 2. The values of $\mathcal{K}_{I\text{-}II}$ for each growth step, $P_i \rightleftharpoons P_{i+1}$, and for each simulation instance are displayed in Fig. 9. As can be seen, $\mathcal{K}_{I\text{-}II}$ is approaching unity shortly after the beginning of the simulation. It should be noted that $\mathcal{K}_I$ accounts for both reactions (Ia) and (Ib), with the latter having a relatively small contribution at the conditions simulated. Effects of other pertinent reactions—like H abstraction by OH, O, CH₃, etc—can be included into $\mathcal{K}_I$ in a similar manner; however, none of them showed a measurable effect at these conditions; also, the removal of $P_i\bullet$ through oxidation in the soot-forming part of the flame is not significant compared to that by hydrogen, reaction (Ib) and the reverse of (Ia).
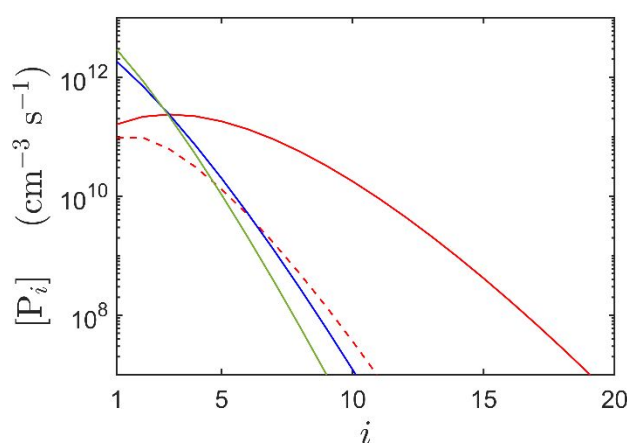
Fig. 8 PAH distributions computed with model (I)-(II) for the midpoint of the flame simulation, t = 5 ms (blue), irreversible nucleation (model 4, solid red), model (4) with $k_f = \beta \times 0.1$ (dashed red), and model (III)-(IV) (green).
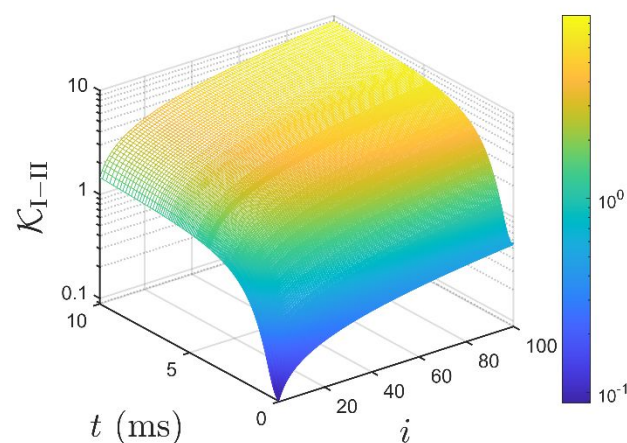
Fig. 9 The reduced equilibrium constant of the two-step growth, (I)-(II).

While step (II) represents reaction between a radical located on one of the zigzag-edge carbons of the PAH cluster, $P_i\bullet$, with one of the C–H sites of a five-member ring of the PAH molecule, P_1, one can consider the "opposite": a reaction between a five-member site of the molecular cluster, P_i, with a zigzag radical of the monomer, $P_1\bullet$,

$$P_1 + H \rightleftharpoons P_1\bullet + H_2 \#(IIIa)$$

This journal is © The Royal Society of Chemistry 20xx

Phys. Chem. Chem. Phys. 2020, **00**, 1-3 | **11**

$$P_1\bullet \ + \ H \ \rightarrow \ P_1 \qquad \#(IIIb)$$
$$P_i \ + \ P_1\bullet \ \rightleftharpoons \ P_{i+1} \ + \ H \ . \#(IV)$$
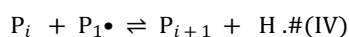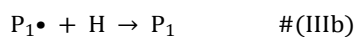
Chemically, reaction (IV) is the same as reaction (II), both are instances of reaction (11) and both end up with the same products and hence have the same reverse rates. Likewise, the forward rate of (IV) is described by the collision efficiency, β, as that of (II). The rate of the (III)-(IV) model, drawn in Fig. 8 as the green line, is somewhat lower, however, than that of (I)-(II). The reason for this is a lower opportunity (frequency) for creation of an edge radical in the case of a single-PAH monomer as compared to that of a polymer cluster.

5 Outlook on the overall soot particle formation

The kinetic analysis of the particle nucleation was performed in this work employing a "linear" polymerization system, eq (3), which models the growth through sequential addition of a monomer. Justification for this approach stems from the primary interest of the present study in the very first steps of the particle inception. The environment of inception is mathematically characterized by the presence of a "strong source" of a monomer, represented by r_0 in the model, and that causes the polymer distribution to assume the Pareto (a power-law[148] or exponential[149]) form. This theoretical prediction for soot-particle nucleation has been confirmed experimentally.[91,95,150,151] Its implication is that the initial stages of nucleation can indeed be represented by eq (3).

The numerical results obtained for the (I)-(II) model in Section 4 demonstrate that such a sequence is capable of producing a meaningful nucleation flux, satisfying requirements A and B enumerated in Section 4.1. Moreover, the average clusters size computed with that model is slightly over 3, (and about 6 with the irreversible case), thus reproducing an important feature of young soot particles, the observed oligomer size of its core structural units.[49,57,58,62,67,68]

As for requirement C, while the formation of the E-bridge does generate non-planarity, its structure is not composed of exactly parallel layers. Such dimers or trimers could be consistent with the very initial particle "seeds", and such dimers have been observed in recent AFM analysis.[51] However, the parallel arrangement of PAH layers is clearly seen in experiment and its interpretations.[51,61,67,68] To rationalize this, one needs to consider that the bridges also undergo reactions—*e.g.*, H-abstraction followed by β-scission. As the time goes on and the bridged oligomer keeps growing at its edges, the initial bridge may transform into another structure, continue PAH-layer growth, or fall apart altogether. Along with this, other bridges may be forming at other PAH-edge sites. Making this assumption may explain the development of the parallel arrangement of PAHs.

The persistent presence of the aliphatic bridges, like the E-bridge in reaction (11), is also in agreement with the experimental observations of aliphatic signals.[95,96] Furthermore, surface condensation[52,71] can now be also explained by a reaction like (11), and the bridge formation in such a model predicts that the aliphatic signal is not only confined to the particle core but is also present at or near the particle surface. The dynamic nature of the bridge formation may lead to variations in the extent of aliphatic component or other characteristics of particle structure at differing formation conditions.

With the increase in the population of the PAH dimers, trimers, etc., collisions among them will start to dominate those of the monomer, thereby building the three-dimensional particle structure. At that point not only reactions forming bridges can play a role, but increasingly other factors, such as higher stability of physical condensation,[55,123] contribution of π-bonding,[124] and polarization-induced forces due to the curvature development in the PAH structure.[85,86]

The essential feature identified by our analysis is that the initial steps of soot particle nucleation are in essence enabled by a HACA-driven mechanism. Specific reactions responsible for the growth step (II and IV of the present study) are most likely broader in scope and some could possibly be more efficient than reaction (11). An interesting possibility is the involvement of five-member rings partially embedded in the aromatic edge. Such rings can be formed in some growth reactions[32,36] and during edge oxidation.[76] These rings and their radicals offer high stability and high electron delocalization.

Another possibility that needs to be considered is the formation of the E-bridge with two-ring PAHs (*i.e.*, naphthalene and acenaphthylene) colliding with each other or with larger PAHs. High concentrations of naphthalene and acenaphthylene have been observed experimentally[152-154] and the HACA theory explains this fact.[3] The two-ring PAH can grow to a larger size while being part of the bridged cluster. However, while the HACA-based growth should be comparable in rate for, say, two- and four-ring PAHs, the destruction (*e.g.*, via H abstraction and β-scission) of the two-ring one is much faster than that of the four-ring aromatics. Also at play is a lower lifetime of the rotationally-excited adduct and lower opportunity for the H-activation for growth of smaller size aromatics compared to the larger ones. The interplay among all these factors will have to be resolved in a future analysis.

Conclusions

The principle conclusion of the present study is that the initial steps of soot particle nucleation are in essence enabled by a HACA-driven mechanism. A rotationally-activated dimer is formed in collision of an aromatic molecule and an aromatic radical and the two react during the lifetime of the rotationally-activated dimer to form a stable, covalently-bonded adduct. A specific reaction identified in the present study forms doubly-bonded bridge, termed E-bridge, between the two PAH moieties. This reaction is rooted in a five-member ring present on the molecule edge.

The energetics and kinetics of several candidate reactions were examined and a most promising one showed to attain a measurable nucleation flux. The proposed model is consistent with other known aspects of soot particle formation, including structural features of the particle self-assembly.

12 | *Phys. Chem. Chem. Phys.* 2020, **00**, 1-3

This journal is © The Royal Society of Chemistry 20xx

Conflicts of interest

There are no conflicts to declare.

Acknowledgements

References

1. B. S. Haynes and H. G. Wagner, Soot formation, *Prog. Energy Combust. Sci.*, 1981, **7**, 229-273.
2. H. G. Wagner, Soot formation in combustion, *Proc. Combust. Inst.*, 1979, **17**, 3-19.
3. M. Frenklach, D. W. Clary, W. C. Gardiner, Jr. and S. E. Stein, Detailed kinetic modeling of soot Formation in shock-tube pyrolysis of acetylene, *Proc. Combust. Inst.*, 1985, **20**, 887-901.
4. S. E. Stein and A. Fahr, High-temperature stabilities of hydrocarbons, *J. Phys. Chem.*, 1985, **89**, 3714-3725.
5. M. Frenklach, Reaction mechanism of soot formation in flames, *Phys. Chem. Chem. Phys.*, 2002, **4**, 2028–2037.
6. R. Rao and M. Esposito, Nonequilibrium thermodynamics of chemical reaction networks: wisdom from stochastic thermodynamics, *Phys. Rev. X*, 2016, **6**, 041064.
7. M. Frenklach, On the driving force of PAH production, *Proc. Combust. Inst.*, 1988, **22**, 1075-1082.
8. A. M. Mebel, Y. Georgievskii, A. W. Jasper and S. J. Klippenstein, Temperature- and pressure-dependent rate coefficients for the HACA pathways from benzene to naphthalene, *Proc. Combust. Inst.*, 2017, **36**, 919-926.
9. M. Frenklach, R. I. Singh and A. M. Mebel, On the low-temperature limit of HACA, *Proc. Combust. Inst.*, 2019, **37**, 969-976.
10. G. Porter, Carbon formation in the combustion wave, *Proc. Combust. Inst.*, 1953, **4**, 248-252.
11. S. J. Harris and A. M. Weiner, Chemical kinetics of soot particle growth, *Annu. Rev. Phys. Chem.*, 1985, **36**, 31-52.
12. M. Frenklach, D. W. Clary, W. C. Gardiner, Jr. and S. E. Stein, Effect of fuel structure on pathways to soot, *Proc. Combust. Inst.*, 1988, **21**, 1067–1076.
13. M. Frenklach, T. Yuan and M. K. Ramachandra, Soot formation in binary hydrocarbon mixtures, *Energy Fuels*, 1988, **2**, 462-480.
14. Y. Yoshihara, A. Kazakov, H. Wang and M. Frenklach, Reduced mechanism of soot formation—Application to natural gas-fueled Diesel combustion, *Proc. Combust. Inst.*, 1994, **25**, 941-948.
15. J. Appel, H. Bockhorn and M. Frenklach, Kinetic modeling of soot formation with detailed chemistry and physics: Laminar premixed flames of C$_2$ hydrocarbons., *Combust. Flame*, 2000, **121**, 122–136.
16. M. Frenklach and W. C. Gardiner, Representation of multistage mechanisms in detailed computer modeling of polymerization kinetics, *J. Phys. Chem.*, 1984, **88**, 6263-6266.
17. M. Frenklach, Computer modeling of infinite reaction sequences: A chemical lumping, *Chem. Eng. Sci.*, 1985, **40**, 1843-1849.
18. B. Shukla and M. Koshi, A highly efficient growth mechanism of polycyclic aromatic hydrocarbons, *Phys. Chem. Chem. Phys.*, 2010, **12**, 2427-2437.
19. B. Shukla and M. Koshi, Comparative study on the growth mechanisms of PAHs, *Combust. Flame*, 2011, **158**, 369-375.
20. B. Shukla and M. Koshi, A novel route for PAH growth in HACA based mechanisms, *Combust. Flame*, 2012, **159**, 3589-3596.
21. B. Shukla, A. Miyoshi and M. Koshi, Role of methyl radicals in the growth of PAHs, *J. Am. Soc. Mass Spectrom.*, 2010, **21**, 534-544.
22. N. Hansen, M. Schenk, K. Moshammer and K. Kohse-Höinghaus, Investigating repetitive reaction pathways for the formation of polycyclic aromatic hydrocarbons in combustion processes, *Combust. Flame*, 2017, **180**, 250-261.
23. A. Raj, M. J. Al Rashidi, S. H. Chung and S. M. Sarathy, PAH growth initiated by propargyl addition: mechanism development and computational kinetics, *J. Phys. Chem. A*, 2014, **118**, 2865-2885.
24. E. Georganta, R. K. Rahman, A. Raj and S. Sinha, Growth of polycyclic aromatic hydrocarbons (PAHs) by methyl radicals: Pyrene formation from phenanthrene, *Combust. Flame*, 2017, **185**, 129-141.
25. P. Liu, Y. Zhang, Z. Li, A. Bennett, H. Lin, S. M. Sarathy and W. L. Roberts, Computational study of polycyclic aromatic hydrocarbons growth by vinylacetylene addition, *Combust. Flame*, 2019, **202**, 276-291.
26. M. Frenklach, C. A. Schuetz and J. Ping, Migration mechanism of aromatic-edge growth, *Proc. Combust. Inst.*, 2005, **30**, 1389-1396.
27. U. Bonne, K. H. Homann and H. G. Wagner, Carbon formation in premixed flames, *Proc. Combust. Inst.*, 1965, **10**, 503-512.
28. K. H. Homann and H. G. Wagner, Some new aspects of the mechanism of carbon formation in premixed flames, *Proc. Combust. Inst.*, 1967, **11**, 371-379.
29. K. H. Homann, 1986, Personal discussion with MF.
30. K. O. Johansson, M. P. Head-Gordon, P. E. Schrader, K. R. Wilson and H. A. Michelsen, Resonance-stabilized hydrocarbon-radical chain reactions may explain soot inception and growth, *Science*, 2018, **361**, 997-1000.
31. A. Violi, Cyclodehydrogenation reactions to cyclopentafused polycyclic aromatic hydrocarbons, *J. Phys. Chem. A*, 2005, **109**, 7781-7787.
32. R. Whitesides, D. Domin, R. Salomón-Ferrer, W. A. Lester Jr and M. Frenklach, Embedded-ring migration on graphene zigzag edge, *Proc. Combust. Inst.*, 2009, **32**, 577–583.
33. R. Whitesides, D. Domin, R. Salomón-Ferrer, W. A. Lester, Jr. and M. Frenklach, Graphene layer growth chemistry: Five- and six-member ring flip reaction, *J. Phys. Chem. A*, 2008, **112**, 2125–2130.
34. R. Whitesides, A. C. Kollias, D. Domin, W. A. Lester Jr and M. Frenklach, Graphene layer growth: Collision of migrating five-member rings, *Proc. Combust. Inst.*, 2007, **31**, 539–546.
35. X. You, R. Whitesides, D. Zubarev, W. A. Lester Jr and M. Frenklach, Bay-capping reactions: kinetics and influence on graphene-edge growth, *Proc. Combust. Inst.*, 2011, **33**, 685–692.
36. R. Whitesides and M. Frenklach, Detailed kinetic Monte Carlo simulations of graphene-edge growth, *J. Phys. Chem. A*, 2010, **114**, 689–703.
37. R. Whitesides and M. Frenklach, Effect of reaction kinetics on graphene-edge morphology and composition, *Z. Phys. Chem.*, 2015, **229**, 597-614.

This journal is © The Royal Society of Chemistry 20xx

Phys. Chem. Chem. Phys. 2020, **00**, 1-3 | **13**

38. E. K. Y. Yapp, C. G. Wells, J. Akroyd, S. Mosbach, R. Xu and M. Kraft, Modelling PAH curvature in laminar premixed flames using a detailed population balance model, *Combust. Flame*, 2017, **176**, 172-180.

39. J. D. Bittner and J. B. Howard, Composition profiles and reaction mechanisms in a near-sooting premixed benzene/oxygen/argon flame, *Proc. Combust. Inst.*, 1981, **18**, 1105-1116.

40. K. H. Homann, Formation of large molecules, particulates and ions in premixed hydrocarbon flames; progress and unresolved questions, *Proc. Combust. Inst.*, 1985, **20**, 857-870.

41. K.-H. Homann, Fullerenes and soot formation— New pathways to large particles in flames, *Angew. Chem. Int. Ed.*, 1998, **37**, 2434-2451.

42. R. L. Vander Wal, A. J. Tomasek, K. Street, D. R. Hull and W. K. Thompson, Carbon nanostructure examined by lattice fringe analysis of high-resolution transmission electron microscopy images, *Appl. Spectroscopy*, 2004, **58**, 230-237.

43. P. D. Teini, D. M. A. Karwat and A. Atreya, Observations of nascent soot: Molecular deposition and particle morphology, *Combust. Flame*, 2011, **158**, 2045-2055.

44. J. Cain, A. Laskin, M. R. Kholghy, M. J. Thomson and H. Wang, Molecular characterization of organic content of soot along the centerline of a coflow diffusion flame, *Phys. Chem. Chem. Phys.*, 2014, **16**, 25862-25875.

45. Y. Matsukawa, K. Ono, K. Dewa, A. Watanabe, Y. Saito, Y. Matsushita, H. Aoki, K. Era, T. Aoki and T. Yamaguchi, Reaction pathway for nascent soot in ethylene pyrolysis, *Combust. Flame*, 2016, **167**, 248-258.

46. P. Desgroux, A. Faccinetto, X. Mercier, T. Mouton, D. Aubagnac Karkar and A. El Bakali, Comparative study of the soot formation process in a "nucleation" and a "sooting" low pressure premixed methane flame, *Combust. Flame*, 2017, **184**, 153-166.

47. K. O. Johansson, T. Dillstrom, P. Elvati, M. F. Campbell, P. E. Schrader, D. M. Popolan-Vaida, N. K. Richards-Henderson, K. R. Wilson, A. Violi and H. A. Michelsen, Radical–radical reactions, pyrene nucleation, and incipient soot formation in combustion, *Proc. Combust. Inst.*, 2017, **36**, 799-806.

48. F. Schulz, M. Commodo, K. Kaiser, G. De Falco, P. Minutolo, G. Meyer, A. D`Anna and L. Gross, Insights into incipient soot formation by atomic force microscopy, *Proc. Combust. Inst.*, 2019, **37**, 885-892.

49. M. L. Botero, Y. Sheng, J. Akroyd, J. Martin, J. A. H. Dreyer, W. Yang and M. Kraft, Internal structure of soot particles in a diffusion flame, *Carbon*, 2019, **141**, 635-642.

50. C. Irimiea, A. Faccinetto, X. Mercier, I.-K. Ortega, N. Nuns, E. Therssen, P. Desgroux and C. Focsa, Unveiling trends in soot nucleation and growth: When secondary ion mass spectrometry meets statistical analysis, *Carbon*, 2019, **144**, 815-830.

51. M. Commodo, K. Kaiser, G. De Falco, P. Minutolo, F. Schulz, A. D'Anna and L. Gross, On the early stages of soot formation: Molecular structure elucidation by high-resolution atomic force microscopy, *Combust. Flame*, 2019, **205**, 154-164.

52. M. Frenklach and H. Wang, Detailed modeling of soot particle nucleation and growth, *Proc. Combust. Inst.*, 1991, **23**, 1559-1566.

53. T. Mitra, T. Zhang, A. D. Sediako and M. J. Thomson, Understanding the formation and growth of polycyclic aromatic hydrocarbons (PAHs) and young soot from n-dodecane in a sooting laminar coflow diffusion flame, *Combust. Flame*, 2019, **202**, 33-42.

54. E. M. Adkins, J. A. Giaccai and J. H. Miller, Computed electronic structure of polynuclear aromatic hydrocarbon agglomerates, *Proc.Combust. Inst.*, 2017, **36**, 957-964.

55. M. L. Botero, E. M. Adkins, S. González-Calera, H. Miller and M. Kraft, PAH structure analysis of soot in a non-premixed flame using high-resolution transmission electron microscopy and optical band gap analysis, *Combust. Flame*, 2016, **164**, 250-258.

56. M. Frenklach and L. B. Ebert, Comment on the proposed role of spheroidal carbon clusters in soot formation, *J. Phys. Chem.*, 1988, **92**, 561-563.

57. H. B. Palmer and C. F. Cullis, The formation of carbon from gases, in *Chemistry and Physics of Carbon*, ed. P. L. Walker, Marcel Dekker, New York, 1965, vol. 1, pp. 265-325.

58. F. A. Heckman and D. F. Harling, Progressive oxidation of selected particles of carbon black: Further evidence for a new microstructural model, *Rubber Chem. Technol.*, 1966, **39**, 1-13.

59. J.-B. Donnet, Fifty years of research and progress on carbon black, *Carbon*, 1994, **32**, 1305-1310.

60. R. Vander Wal, A. Yezerets, N. W. Currier, D. H. Kim and C. M. Wang, HRTEM study of diesel soot collected from diesel particulate filters, *Carbon*, 2007, **45**, 70-77.

61. J. Happold, H.-H. Grotheer and M. Aigner, Soot precursors consisting of stacked pericondensed PAHs, in *Combustion Generated Fine Carbon Particles* eds. H. Bockhorn, A. D'Anna, A. F. Sarofim and H. Wang, Karlsruhe University Karlsruhe, Germany, 2009, pp. 275-285.

62. C. S. Wang, N. C. Bartelt, R. Ragan and K. Thürmer, Revealing the molecular structure of soot precursors, *Carbon*, 2018, **129**, 537-542.

63. K. Wan, D. Chen and H. Wang, On imaging nascent soot by transmission electron microscopy, *Combust. Flame*, 2018, **198**, 260-266.

64. M. Wang, Q. Tang, J. Mei and X. You, On the effective density of soot particles in premixed ethylene flames, *Combust. Flame*, 2018, **198**, 428-435.

65. H. Jiang, T. Li, Y. Wang, P. He and B. Wang, The evolution of soot morphology and nanostructure along axial direction in diesel spray jet flames, *Combust. Flame*, 2019, **199**, 204-212.

66. V. B. Malmborg, A. C. Eriksson, S. Török, Y. Zhang, K. Kling, J. Martinsson, E. C. Fortner, L. Gren, S. Kook, T. B. Onasch, P.-E. Bengtsson and J. Pagels, Relating aerosol mass spectra to composition and nanostructure of soot particles, *Carbon*, 2019, **142**, 535-546.

67. K. Bowal, J. W. Martin and M. Kraft, Partitioning of polycyclic aromatic hydrocarbons in heterogeneous clusters, *Carbon*, 2019, **143**, 247-256.

68. F. Carbone, M. R. Canagaratna, A. T. Lambe, J. T. Jayne, D. R. Worsnop and A. Gomez, Exploratory analysis of a sooting premixed flame via on-line high resolution (APi–TOF) mass spectrometry, *Proc. Combust. Inst.*, 2019, **37**, 919-926.

69. A. D'Alessio, A. D`Anna, P. Minutolo and I. A. Sgro, Nanoparticles of organic carbon (NOC) formed in flames and their effects in urban atmospheres, in *Combustion Generated Fine Carbon Particles*, eds. H. Bockhorn, A. D'Anna, A. F. Sarofim and H. Wang, KIT Scientific, Karlsruhe, Germany, 2009, pp. 201-227.

70. M. Frenklach, in *Soot Formation in Combustion: An International Round Table Discussion*, eds. H. Jander and H. G. Wagner, Göttingen, 1989, pp. 35-36.

71. M. Frenklach and H. Wang, Detailed mechanism and modeling of soot particle formation, in *Soot Formation in Combustion: Mechanisms and Models*, ed. H. Bockhorn, Springer-Verlag, Heidelberg, 1994, pp. 165-192.

14 | *Phys. Chem. Chem. Phys.* 2020, **00**, 1-3

This journal is © The Royal Society of Chemistry 20xx

72. J. H. Miller, K. C. Smyth and W. G. Mallard, Calculations of the dimerization of aromatic hydrocarbons: Implications for soot formation, *Proc. Combust. Inst.*, 1985, **20**, 1139-1147.

73. H. Sabbah, L. Biennier, S. J. Klippenstein, I. R. Sims and B. R. Rowe, Exploring the role of PAHs in the formation of soot: Pyrene dimerization, *J. Phys. Chem. Lett.*, 2010, **1**, 2962-2967.

74. P. Elvati and A. Violi, Thermodynamics of poly-aromatic hydrocarbon clustering and the effects of substituted aliphatic chains, *Proc. Combust. Inst.*, 2013, **34**, 1837-1843.

75. T. S. Totton, A. J. Misquitta and M. Kraft, A quantitative study of the clustering of polycyclic aromatic hydrocarbons at high temperatures, *Phys. Chem. Chem. Phys.*, 2012, **14**, 4081-4094.

76. M. Frenklach, Z. Liu, R. I. Singh, G. R. Galimova, V. N. Azyazov and A. M. Mebel, Detailed, sterically-resolved modeling of soot oxidation: Role of O atoms, interplay with particle nanostructure, and emergence of inner particle burning, *Combust. Flame*, 2018, **188**, 284-306.

77. A. D. Abid, J. Camacho, D. A. Sheen and H. Wang, Quantitative measurement of soot particle size distribution in premixed flames—The burner-stabilized stagnation flame approach, *Combust. Flame*, 2009, **156**, 1862-1870.

78. H. F. Calcote, Mechanisms of soot nucleaion in flames—A critical review, *Combust. Flame*, 1981, **42**, 215-242.

79. H. F. Calcote, D. B. Olson and D. G. Keil, Are ions important in soot formation?, *Energy & Fuels*, 1988, **2**, 494-504.

80. V. J. Hall-Roberts, A. N. Hayhurst, D. E. Knight and S. G. Taylor, The origin of soot in flames: Is the nucleus or ion?, *Combust. Flame*, 2000, **120**, 578-584.

81. H. Wang, B. Weiner and M. Frenklach, Theoretical study of reaction between phenylvinyleum ion and acetylene, *J. Phys. Chem.*, 1993, **97**, 10364-10371.

82. M. Balthasar, F. Mauss and H. Wang, A computational study of the thermal ionization of soot particles and its effect on their growth in laminar premixed flames, *Combust. Flame*, 2002, **129**, 204-216.

83. D. Chen and H. Wang, Cation–π interactions between flame chemi-ions and aromatic compounds, *Energy & Fuels*, 2017, **31**, 2345-2352.

84. J. W. Martin, R. I. Slavchov, E. K. Y. Yapp, J. Akroyd, S. Mosbach and M. Kraft, The polarization of polycyclic aromatic hydrocarbons curved by pentagon incorporation: The role of the flexoelectric dipole, *J. Phys. Chem. C*, 2017, **121**, 27154-27163.

85. J. W. Martin, K. Bowal, A. Menon, R. I. Slavchov, J. Akroyd, S. Mosbach and M. Kraft, Polar curved polycyclic aromatic hydrocarbons in soot formation, *Proc. Combust. Inst.*, 2019, **37**, 1117-1123.

86. K. Bowal, J. W. Martin, A. J. Misquitta and M. Kraft, Ion-induced soot nucleation using a new potential for curved aromatics, *Combust. Sci. Technol.*, 2019, **191**, 747-765.

87. J. W. Martin, A. Menon, C. T. Lao, J. Akroyd and M. Kraft, Dynamic polarity of curved aromatic soot precursors, *Combust. Flame*, 2019, **206**, 150-157.

88. M. Frenklach, M. K. Ramachandra and R. A. Matula, Soot formation in shock-tube oxidation of hydrocarbons, *Proc. Combust. Inst.*, 1985, **20**, 871-878.

89. A. B. Fialkov, Investigations on ions in flames, *Prog. Energy Combust. Sci.*, 1997, **23**, 399-528.

90. H. R. N. Jones and A. N. Hayhurst, Measurements of the concentrations of positive and negative ions along premixed fuel-rich flames of methane and oxygen, *Combust. Flame*, 2016, **166**, 86-97.

91. J. Camacho, C. Liu, C. Gu, H. Lin, Z. Huang, Q. Tang, X. You, C. Saggese, Y. Li, H. Jung, L. Deng, I. Wlokas and H. Wang, Mobility size and mass of nascent soot particles in a benchmark premixed ethylene flame, *Combust. Flame*, 2015, **162**, 3810-3822.

92. D. Hou, C. S. Lindberg, M. Y. Manuputty, X. You and M. Kraft, Modelling soot formation in a benchmark ethylene stagnation flame with a new detailed population balance model, *Combust. Flame*, 2019, **203**, 56-71.

93. P. Elvati, V. T. Dillstrom and A. Violi, Oxygen driven soot formation, *Proc. Combust. Inst.*, 2017, **36**, 825-832.

94. P. Liu, B. Chen, Z. Li, A. Bennett, S. Sioud, S. M. Sarathy and W. L. Roberts, Evolution of oxygenated polycyclic aromatic hydrocarbon chemistry at flame temperatures, *Combust. Flame*, 2019, **209**, 441-451.

95. B. Öktem, M. P. Tolocka, B. Zhao, H. Wang and M. V. Johnston, Chemical species associated with the early stage of soot growth in a laminar premixed ethylene–oxygen–argon flame, *Combust. Flame*, 2005, **142**, 364-373.

96. K. C. Le, C. Lefumeux, P.-E. Bengtsson and T. Pino, Direct observation of aliphatic structures in soot particles produced in low-pressure premixed ethylene flames via online Raman spectroscopy, *Proc. Combust. Inst.*, 2019, **37**, 869-876.

97. A. Giordana, A. Maranzana and G. Tonachini, Carbonaceous nanoparticle molecular inception from radical addition and van der Waals coagulation of polycyclic aromatic hydrocarbon-based systems. A theoretical study, *J. Phys. Chem. C*, 2011, **115**, 17237-17251.

98. A. V. Krestinin, Detailed modeling of soot formation in hydrocarbon pyrolysis, *Combust. Flame*, 2000, **121**, 513-524.

99. A. Kazakov and M. Frenklach, 1994, unpublished work.

100. Q. Mao, A. C. T. van Duin and K. H. Luo, Formation of incipient soot particles from polycyclic aromatic hydrocarbons: A ReaxFF molecular dynamics study, *Carbon*, 2017, **121**, 380-388.

101. H. Yuan, W. Kong, F. Liu and D. Chen, Study on soot nucleation and growth from PAHs and some reactive species at flame temperatures by ReaxFF molecular dynamics, *Chem. Eng. Sci.*, 2019, **195**, 748-757.

102. M. R. Kholghy, G. A. Kelesidis and S. E. Pratsinis, Reactive polycyclic aromatic hydrocarbon dimerization drives soot nucleation, *Phys. Chem. Chem. Phys.*, 2018, **20**, 10926-10938.

103. I. Fleming, *Molecular orbitals and organic chemical reactions*, Wiley, Chichester, UK, 2009.

104. I. Glassman, *Phenomenological models of soot processes in combustion systems*, Report No. 1450, Princeton University, Princeton, N.J., 1979.

105. M. Frenklach, S. Taki, M. B. Durgaprasad and R. A. Matula, Soot formation in shock-tybe pyrolysis of acetylene, allene, and 1,3-butadiene, *Combust. Flame*, 1983, **54**, 81-101.

106. J. A. Miller and S. J. Klippenstein, The recombination of propargyl radicals and other reactions on a C6H6 potential, *J. Phys. Chem. A*, 2003, **107**, 7783-7799.

107. G. da Silva, J. A. Cole and J. W. Bozzelli, Kinetics of the cyclopentadienyl + acetylene, fulvenallene + H, and 1-ethynylcyclopentadiene + H reactions, *J. Phys. Chem. A*, 2010, **114**, 2275-2283.

108. J. D. Savee, T. M. Selby, O. Welz, C. A. Taatjes and D. L. Osborn, Time- and isomer-resolved measurements of sequential addition of acetylene to the propargyl radical, *J. Phys. Chem. Lett.*, 2015, **6**, 4153-4158.

109. L. Zhao, M. B. Prendergast, R. I. Kaiser, B. Xu, W. Lu, U. Ablikim, M. Ahmed, A. D. Oleinikov, V. N. Azyazov, A. M. Mebel, A. H. Howlader and S. F. Wnuk, Reactivity of the indenyl radical (C_9H_7)

This journal is © The Royal Society of Chemistry 20xx

Phys. Chem. Chem. Phys. 2020, **00**, 1-3 | **15**

with acetylene (C_2H_2) and vinylacetylene (C_4H_4), *ChemPhysChem*, 2019, **20**, 1437-1447.

110. J. H. Miller, The kinetics of polynuclear aromatic hydrocarbon agglomeration in flames, *Proc. Combust. Inst.*, 1990, **23**, 91-98.

111. C. A. Schuetz and M. Frenklach, Nucleation of soot: Molecular dynamics simulations of pyrene dimerization, *Proc. Combust. Inst.*, 2003, **29**, 2307-2314.

112. D. Wong, R. Whitesides, C. A. Schuetz and M. Frenklach, Molecular dynamics simulations of PAH dimerization, in *Combustion Generated Fine Carbon Particles*, eds. H. Bockhorn, A. D'Anna, A. F. Sarofim and H. Wang, KIT Scientific, Karlsruhe, Germany, 2009, pp. 245-255.

113. P. Elvati, K. Turrentine and A. Violi, The role of molecular properties on the dimerization of aromatic compounds, *Proc. Combust. Inst.*, 2019, **37**, 1099-1105.

114. P. Elvati and A. Violi, Homo-dimerization of oxygenated polycyclic aromatic hydrocarbons under flame conditions, *Fuel*, 2018, **222**, 307-311.

115. S. Wu, F. Li, D. Zhang, T. Zhang and G. Guo, Molecular modelling investigations on the possibility of phenanthrene dimers to be the primary nuclei of soot, *Combust. Theory Model.*, 2017, **21**, 1189-1198.

116. M. Balthasar and M. Frenklach, Detailed kinetic modeling of soot aggregate formation in laminar premixed flames, *Combust. Flame*, 2005, **140**, 130-145.

117. J. L. Katz and M. D. Donohue, A kinetic approach to homogeneous nucleation theory, in *Advances in Chemical Physics*, eds. I. Prigogine and S. A. Rice, Wiley, 1979, vol. XL, pp. 137-154.

118. R. Zhang, A. Khalizov, L. Wang, M. Hu and X. W., Nucleation and growth of nanoparticles in the atmosphere, *Chem. Rev.*, 2012, **112**, 1957-2011.

119. S. M. Kathmann, G. K. Schenter, B. C. Garrett, B. Chen and J. I. Siepmann, Thermodynamics and kinetics of nanoclusters controlling gas-to-particle nucleation, *J. Phys. Chem. C*, 2009, **113**, 10354-10370.

120. S. K. Friedlander, *Smoke, Dust, and Haze: Fundamentals of Aerosol Dynamics*, Oxford University, Oxford, UK, 2000.

121. Matlab, http://www.mathworks.com/).

122. D. G. Goodwin, R. L. Speth, H. K. Moffat and B. W. Weber, Cantera: An object-oriented software toolkit for chemical kinetics, thermodynamics, and transport processes, https://cantera.org/).

123. J. D. Herdman and J. H. Miller, Intermolecular potential calculations for polynuclear aromatic hydrocarbon clusters, *J. Phys. Chem. A*, 2008, **112**, 6249-6256.

124. H. Wang, Formation of nascent soot and other condensed-phase materials in flames, *Proc. Combust. Inst.*, 2011, **33**, 41-67.

125. T. Yang, R. I. Kaiser, T. P. Troy, B. Xu, O. Kostko, M. Ahmed, A. M. Mebel, M. V. Zagidullin and V. N. Azyazov, HACA's heritage: A free-radical pathway to phenanthrene in circumstellar envelopes of asymptotic giant branch stars, *Angew. Chem. Int. Ed.*, 2017, **56**, 4515-4519.

126. A. D. Becke, Density-functional thermochemistry. III. The role of exact exchange *J. Chem. Phys.*, 1993, **98**, 5648–5652.

127. C. T. Lee, W. T. Yang and R. G. Parr, Development of the Colle-Salvetti correlation-energy formula into a functional of the electron density, *Phys. Rev. B*, 1988, **37**, 785–789.

128. A. G. Baboul, L. A. Curtiss, P. C. Redfern and K. Raghavachari, Gaussian-3 theory using density functional geometries and zero point energies, *J. Chem. Phys.*, 1999, **110**, 7650-7657.

129. L. A. Curtiss, K. Raghavachari, P. C. Redfern, A. G. Baboul and J. A. Pople, Gaussian-3 theory using coupled cluster energies, *Chem. Phys. Lett.*, 1999, **314**, 101–107.

130. Y. Zhao and D. G. Truhlar, Density functionals with broad applicability in chemistry, *Acc. Chem. Res.*, 2008, **41**, 157–167.

131. J.-D. Chai and M. Head-Gordon, Long-range corrected hybrid density functionals with damped atom-atom dispersion corrections, *Phys. Chem. Chem. Phys.*, 2008, **10**, 6615-6620.

132. S. Grimme, Semiempirical hybrid density functional with perturbative second-order correlation, *J. Chem. Phys.*, 2006, **124**, 034108.

133. L. Goerigk and S. Grimme, Efficient and accurate double-hybrid-meta-GGA Density Functionals—Evaluation with the extended GMTKN30 database for general main group thermochemistry, kinetics, and noncovalent interactions, *J. Chem. Theory Comput.*, 2011, **7**, 291-309.

134. S. Grimme, S. Ehrlich and L. Goerigk, Effect of the damping function in dispersion corrected density functional theory, *J. Comp. Chem.*, 2011, **32**, 1456-1465.

135. T. H. Dunning, Gaussian basis sets for use in correlated molecular calculations. I. The atoms boron through neon and hydrogen, *J. Chem. Phys.*, 1989, **90**, 1007-1023.

136. M. J. Frisch, G. W. Trucks, H. B. Schlegel, G. E. Scuseria, M. A. Robb, J. R. Cheeseman, G. Scalmani, V. Barone, B. Mennucci, G. A. Petersson, H. Nakatsuji, M. Caricato, X. Li, H. P. Hratchian, A. F. Izmaylov, J. Bloino, G. Zheng, J. L. Sonnenberg, M. Hada, M. Ehara, K. Toyota, R. Fukuda, J. Hasegawa, M. Ishida, T. Nakajima, Y. Honda, O. Kitao, H. Nakai, T. Vreven, J. J. A. Montgomery, J. E. Peralta, F. Ogliaro, M. Bearpark, J. J. Heyd, E. Brothers, K. N. Kudin, V. N. Staroverov, T. Keith, R. Kobayashi, J. Normand, K. Raghavachari, A. Rendell, J. C. Burant, S. S. Iyengar, J. Tomasi, M. Cossi, N. Rega, J. M. Millam, M. Klene, J. E. Knox, J. B. Cross, V. Bakken, C. Adamo, J. Jaramillo, R. Gomperts, R. E. Stratmann, O. Yazyev, A. J. Austin, R. Cammi, C. Pomelli, J. W. Ochterski, R. L. Martin, K. Morokuma, V. G. Zakrzewski, G. A. Voth, P. Salvador, J. J. Dannenberg, S. Dapprich, A. D. Daniels, O. Farkas, J. B. Foresman, J. V. Ortiz, J. Cioslowski and D. J. Fox, 2010, Gaussian 09.

137. H.-J. Werner, P. J. Knowles, G. Kinizia, F. R. Manby, M. Schutz, P. Celani, T. Korona and R. Lindh, 2010, MOLPRO, version 2010.1.

138. Y. Georgievskii, J. A. Miller, M. P. Burke and S. J. Klippenstein, Reformulation and solution of the master equation for multiple-well chemical reactions, *J. Phys. Chem. A*, 2013, **117**, 12146-12154.

139. Y. Georgievskii and S. J. Klippenstein, 2015, Master Equation System Solver (MESS), available on line at https://github.com/PACChem/MESS.

140. H. Wang and M. Frenklach, Transport properties of polycyclic aromatic hydrocarbons for flame modeling, *Combust. Flame*, 1994, **96**, 163–170.

141. A. Vishnyakov, P. G. Debenedetti and A. V. Neimark, Statistical geometry of cavities in a metastable confined fluid, *Phys. Rev. E*, 2000, **62**, 538-544.

142. A. V. Neimark, P. I. Ravikovitch and A. Vishnyakov, Adsorption hysteresis in nanopores, *Phys. Rev. E*, 2000, **62**, R1493-R1496.

143. J. Troe, Theory of thermal unimolecular reactions at low pressures. I. Solutions of the master equation, *J. Chem. Phys.*, 1977, **66**, 4745-4757.

144. A. W. Jasper and J. A. Miller, Theoretical unimolecular kinetics for CH_4 + M ⇄ CH_3 + H + M in eight baths, M = He, Ne, Ar, Kr, H_2, N_2, CO, and CH_4, *J. Phys. Chem. A*, 2011, **115**, 6438-6455.

16 | *Phys. Chem. Chem. Phys.* 2020, **00**, 1-3

This journal is © The Royal Society of Chemistry 20xx

145. C. S. Carmer, B. Weiner and M. Frenklach, Molecular dynamics with combined quantum and empirical potentials: C_2H_2 adsorption on Si(100), *J. Chem. Phys.*, 1993, **99**, 1356-1372.
146. A. S. Semenikhin, A. S. Savchenkova, I. V. Chechet, S. G. Matveev, Z. Liu, M. Frenklach and A. M. Mebel, Rate constants for H abstraction from benzo(a)pyrene and chrysene: a theoretical study, *Phys. Chem. Chem. Phys.*, 2017, **19**, 25401-25413.
147. L. B. Harding, Y. Georgievskii and S. J. Klippenstein, Predictive theory for hydrogen atom–Hydrocarbon radical association kinetics, *J. Phys. Chem. A*, 2005, **109**, 4646-4656.
148. M. Frenklach and S. J. Harris, Aerosol dynamics modeling using the method of moments, *J. Colloid Interface Sci.*, 1987, **118**, 252-261.
149. M. Frenklach, Dynamics of discrete distribution for Smoluchowski coagulation model, *J. Colloid Interface Sci.*, 1985, **108**, 237-242.
150. C. Gu, H. Lin, J. Camacho, B. Lin, C. Shao, R. Li, H. Gu, B. Guan, Z. Huang and H. Wang, Particle size distribution of nascent soot in lightly and heavily sooting premixed ethylene flames, *Combust. Flame*, 2016, **165**, 177-187.
151. M. Lucchesi, A. Abdelgadir, A. Attili and F. Bisetti, Simulation and analysis of the soot particle size distribution in a turbulent nonpremixed flame, *Combust. Flame*, 2017, **178**, 35-45.
152. H. Bockhorn, F. Fetting and H. W. Wenz, Investigation of the formation of high molecular hydrocarbons and soot in premixed hydrocarbon-oxygen flames, *Ber. Bunsenges. Phys. Chem.*, 1983, **87**, 1067-1073.
153. M. Wartel, J. F. Pauwels, P. Desgroux and X. Mercier, Quantitative measurement of naphthalene in low-pressure flames by jet-cooled laser-induced fluorescence, *Appl. Phys. B*, 2010, **100**, 933-943.
154. K. Gleason, F. Carbone, A. J. Sumner, B. D. Drollette, D. L. Plata and A. Gomez, A novel method for spatially-resolved quantitation of large polycyclic aromatic hydrocarbons in laminar sooting flames, presented at the 11th U. S. National Combustion Meeting, Pasadena, California, March 24-27, 2019.

This journal is © The Royal Society of Chemistry 20xx

Phys. Chem. Chem. Phys. 2020, **00**, 1-3 | **17**

A table of contents entry.

graphic
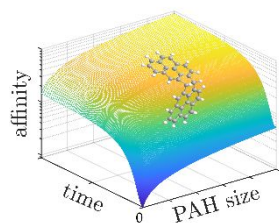
Sentence:

New ideas and theoretical results offer a solution to soot particle inception following critical examination of prior proposals.